La Tomografia sismica in velocità, attenuazione e scattering e l'immagine della struttura dei vulcani.

Edoardo Del Pezzo

Istituto Nazionale di Geofisica e Vulcanologia, sezione di Napoli "Osservatorio Vesuviano"

30° convegno nazionale GNGTS, 14-17 novembre 2011. Trieste

Why high resolution seismic tomography in volcanoes:

- to explore the presence and location of partially molten materials in the earth crust (magma chambers).
- to constrain eruption models.
- to contribute to the definition of eruption risk.

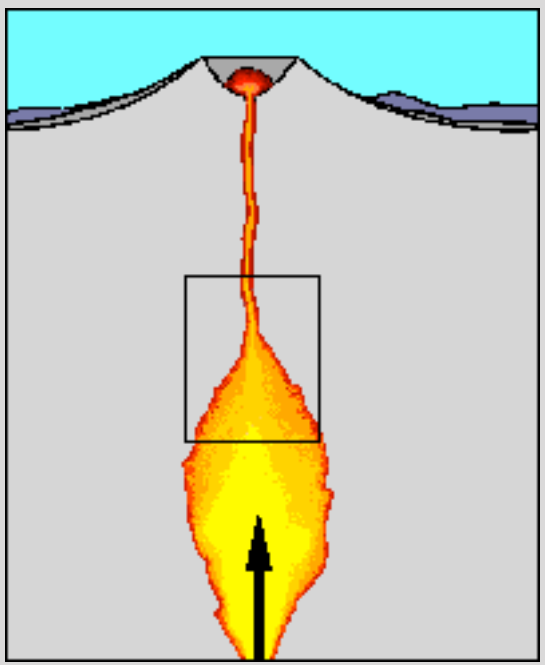

We expect to obtain 3-D images reflecting the concept expressed in the left-side scheme, taken from USGS web:

http://volcanoes.usgs.gov/images/pglossary/magma.php

Which kind of seismic attributes should be taken into account:

- Travel time Tomography: Arrival times of the main phases.
- Attenuation Tomography: Seismic radiation spectra.
- Scattering Tomography: Energy coda envelopes and/or array measurements of slowness vectors associated with coherent phases in the coda.

In this seminar:
a) A brief review of the results from travel time tomography at Mt. Vesuvius ed at Campi Flegrei.
b) New approaches: (passive) attenuation and scattering tomography.
c) Results obtained (passive attenuation and scattering) at Mt. Vesuvio and Campi Flegrei described in the following bibliography:

De Siena, L., Del Pezzo, E. and Bianco, F. A scattering image of Campi Flegrei from the autocorrelation functions of velocity tomograms. Geophysical Journal International (2011) vol. 184 (3) pp. 1304-1310

De Siena, L., Del Pezzo, E. and Bianco, F. Seismic attenuation imaging of Campi Flegrei: Evidence of gas reservoirs, hydrothermal basins, and feeding systems. Journal of Geophysical Research-Solid Earth (2010) vol. 115 pp. B09312

Battaglia, J., Zollo, A., Virieux, J., Dello Iacono, D. Merging active and passive data sets in traveltime tomography: The case study of Campi Flegrei caldera (Southern Italy). Geophysical Prospecting (2008) vol. 56 (4) pp. 555-573

Tramelli, A., Del Pezzo, E., Galluzzo, D. and Fehler, M.C. Anomalous character of the coda envelopes on Mt Vesuvius explained in terms of depth dependent Q. Geophysical Journal International (2010) vol. 181 (2) pp. 926-934

De Siena, L., Del Pezzo, E., Bianco, F., Tramelli, A. Multiple resolution seismic attenuation imaging at Mt. Vesuvius. Physics of The Earth and Planetary Interiors (2009) vol. 173 (1-2) pp. 17-32

Scarpa, R., Tronca, F., Bianco, F., Del Pezzo, E. High resolution velocity structure beneath Mount Vesuvius from seismic array data. Geophysical Research Letters (2002)

The ordinary "travel time tomography"

Pioneer papers

Tecniques (metods ACH - Velinv):
Aki, Huseby ,Christofferson and Powell, 1974 EOS Trans. Am. Geophys. Un. 56:1145
Crosson, RS, 1976. J. Geophys. Res., 81, 3036-3046
Aki, Christofferson and Huseby, 1977 J. Geophys. Res. 82, 277-296

Applications to volcanoes (travel time residuals):
Iyer, 1975 Nature. 253, 425-427 (Yellowstone caldera)

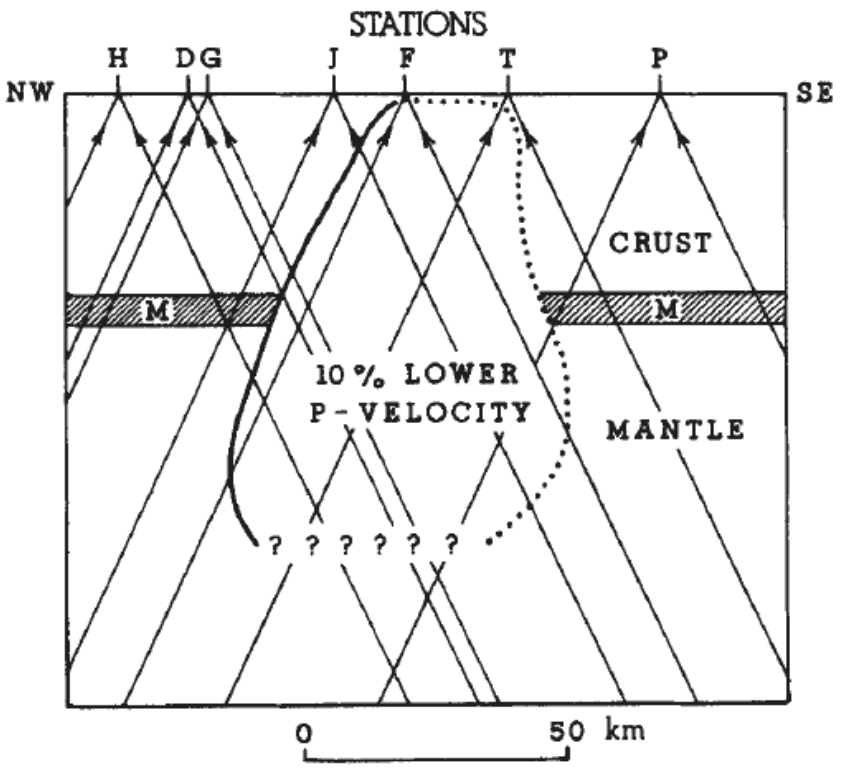

Fig. 3 North-westerly trending vertical cross section of the low velocity body that possibly explains the travel time delay pattern. The boundary of the body is shown by a heavy solid line where well constrained by the data, by a dotted line where only poorly constrained, and by question marks where the boundary cannot be determined. Arrows, schematic ray paths for events in the north-western and south-eastern azimuths. Width of the dark shaded band (Moho) indicates uncertainty in crustal thickness[13].

Applications to volcanoes (metod ACH):
Ellsworth and Koyanagi, 1977 J. Geophys. Res. 82, 5379-5394
(Kilauea, Hawaii

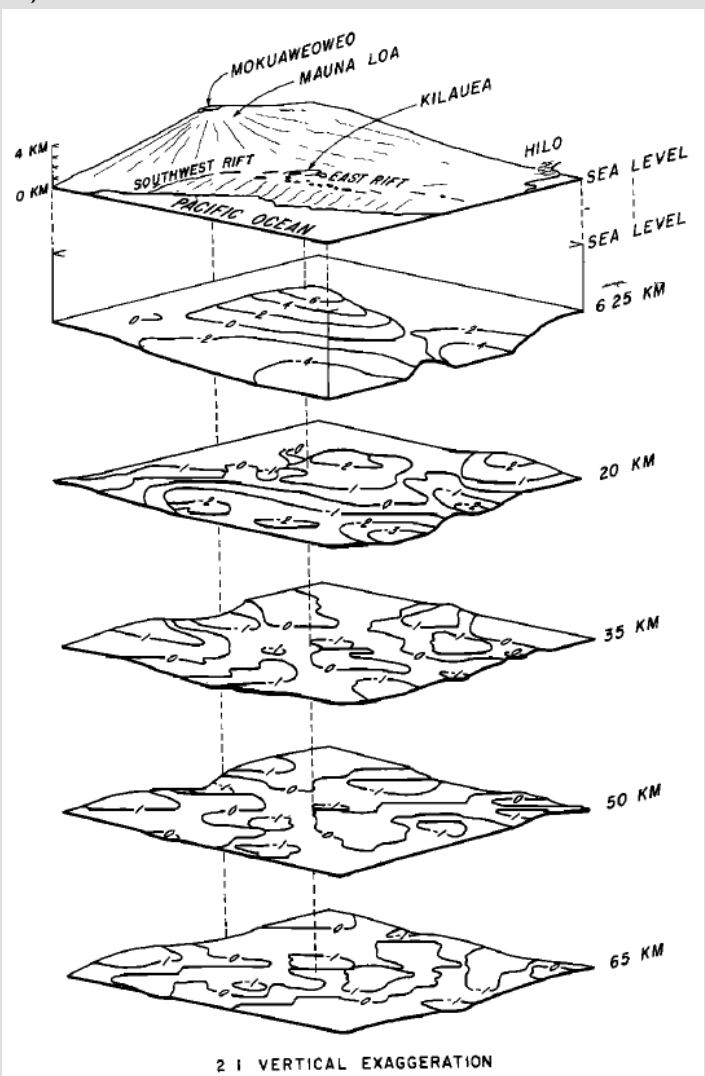

Fig. 11. Perspective view of smoothed velocity perturbations displayed as a raised relief surface. Compressional wave velocity contoured at 2% intervals in crust and 1% intervals in mantle.

Results from a passive P- travel time tomography study at Mt. Vesuvio (Scarpa et al., 2002)

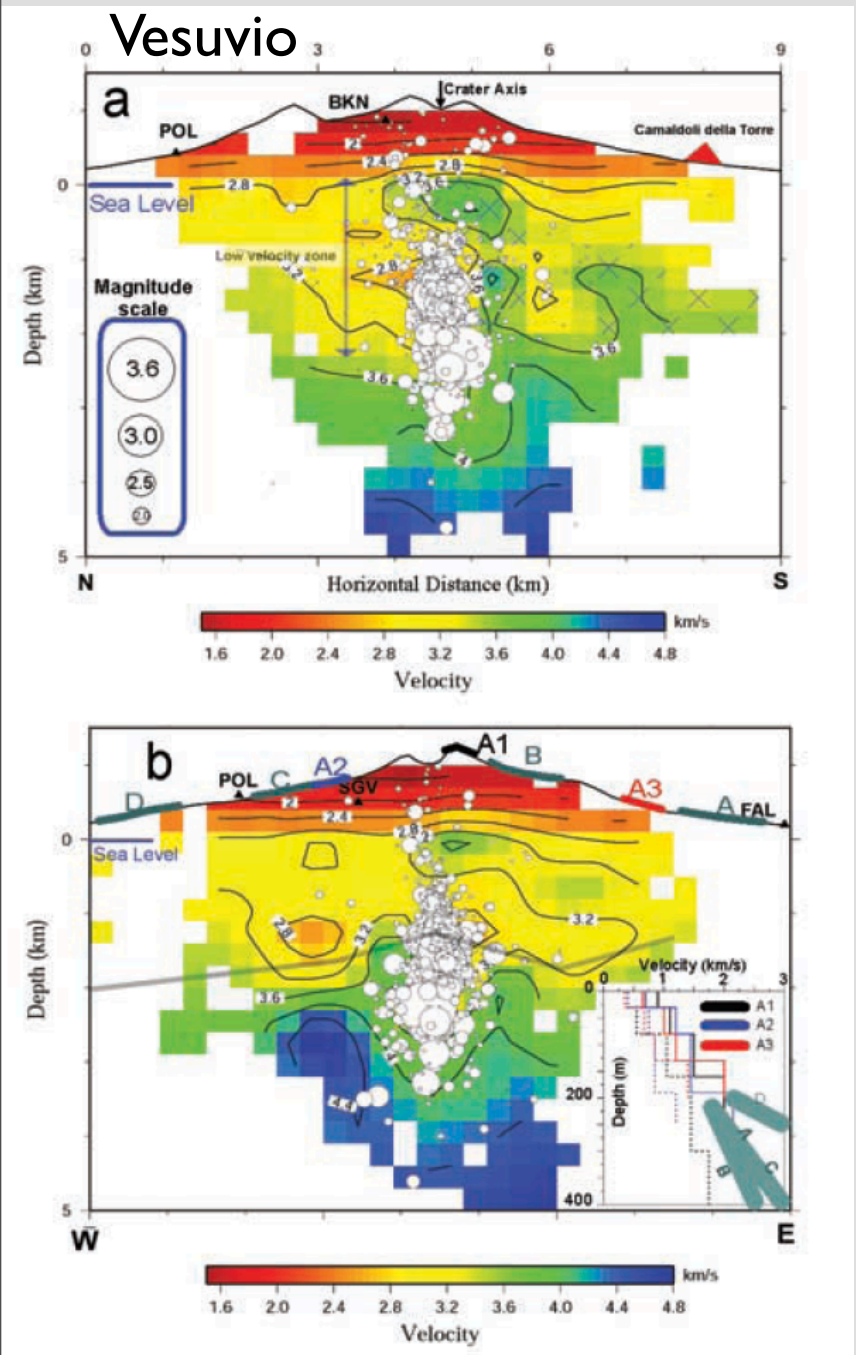

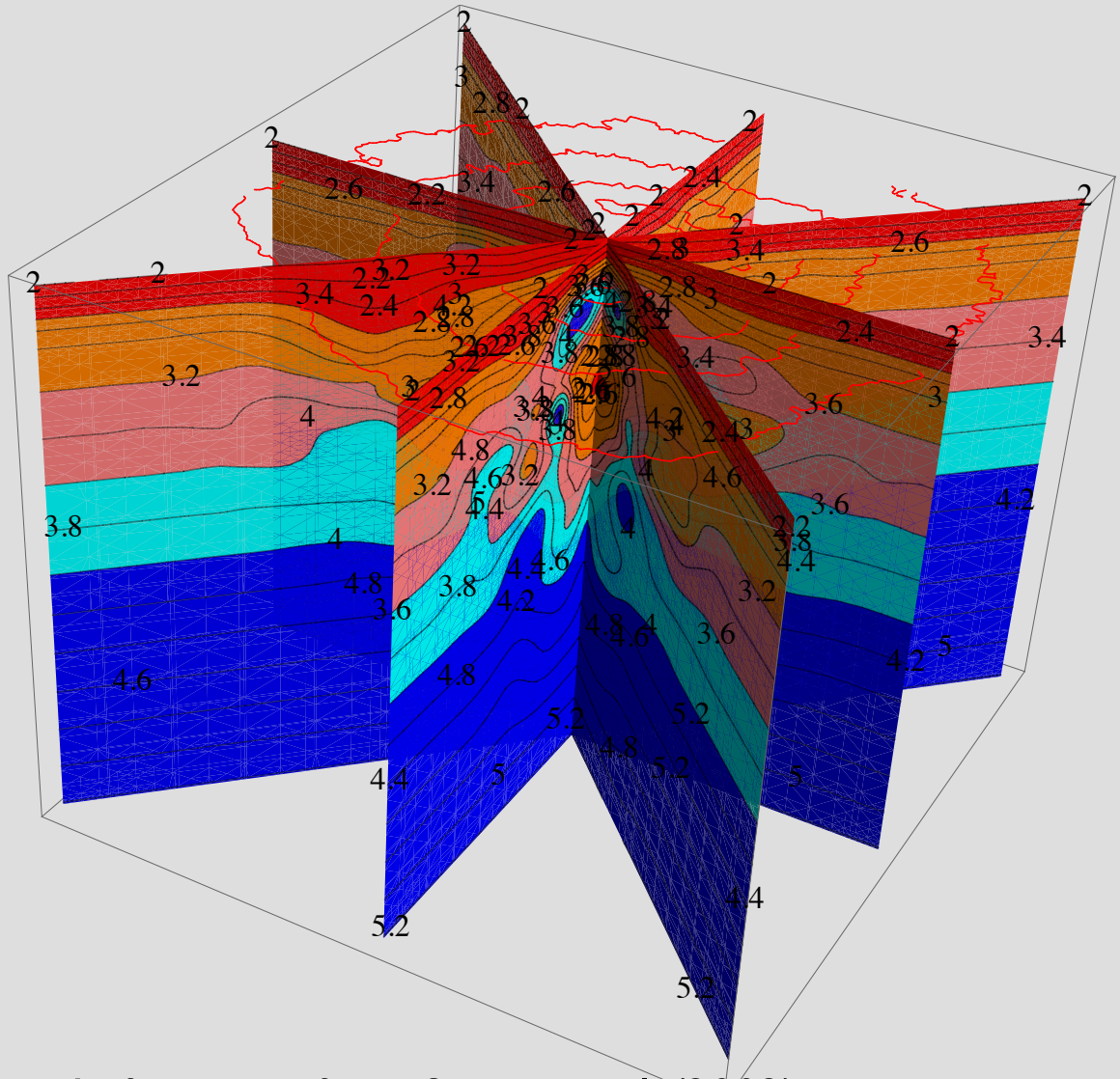

Left: images from Scarpa et al. (2002)
Up: Spatially interpolated Vp values done using MATHEMATICA

Other interesting images of the same volcano can be found in the RISSC lab home page (University of Naples, INGV and AMRA) (G. Iannaccone and A. Zollo coordinators) http://www.rissclab.unina.it/ and in a number of papers by De Natale and co-workers.
The main projects are TOMOVES (P. Gasparini, coordinator) and DPC-INGV "Vesuvio"

Results from an active/passive P- and S- travel time tomography study at Campi Flegrei (Battaglia et al., 2008)

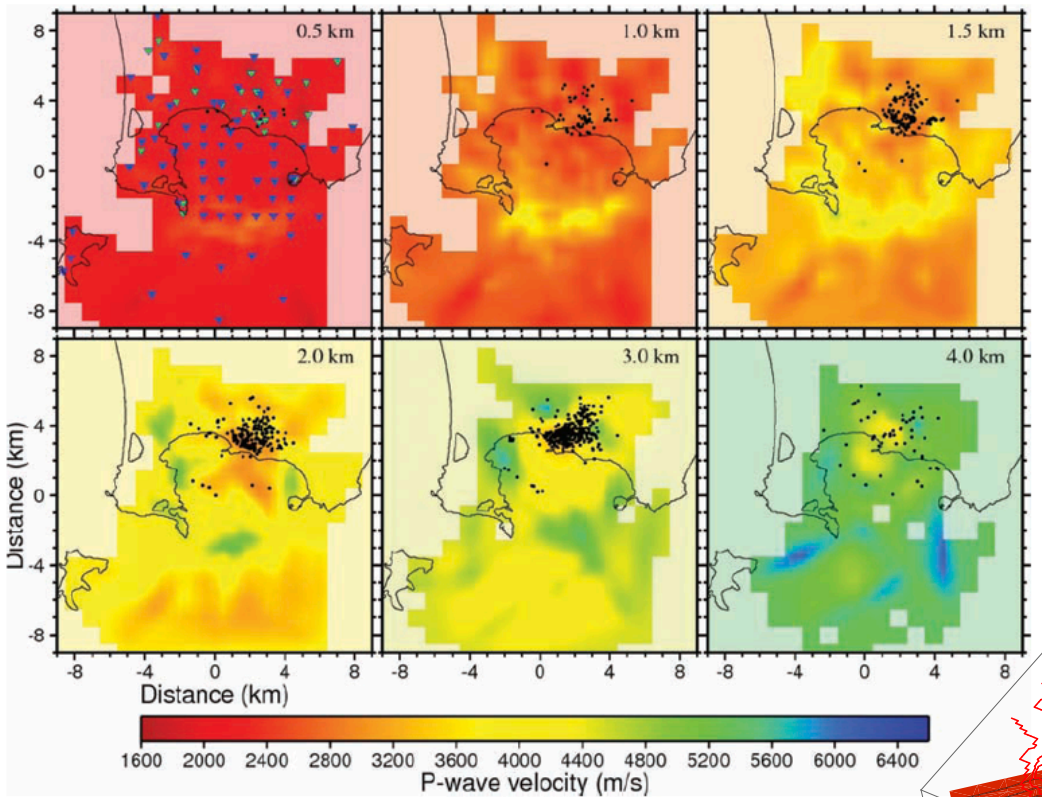

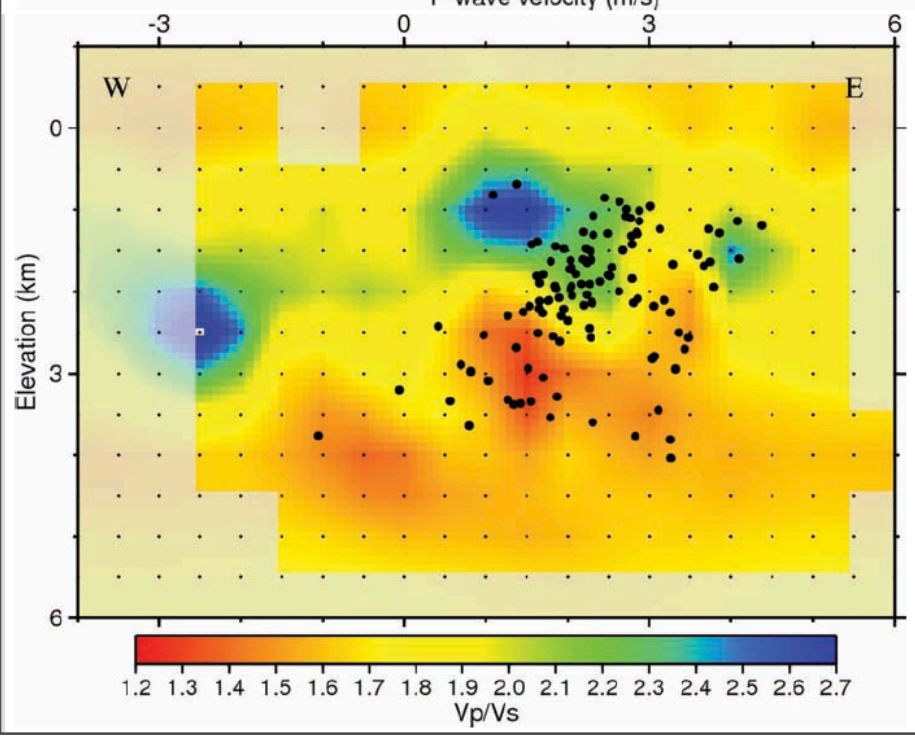

Left: images from Battaglia et al. (2008)

Down: Spatially interpolated Vp values done using MATHEMATICA

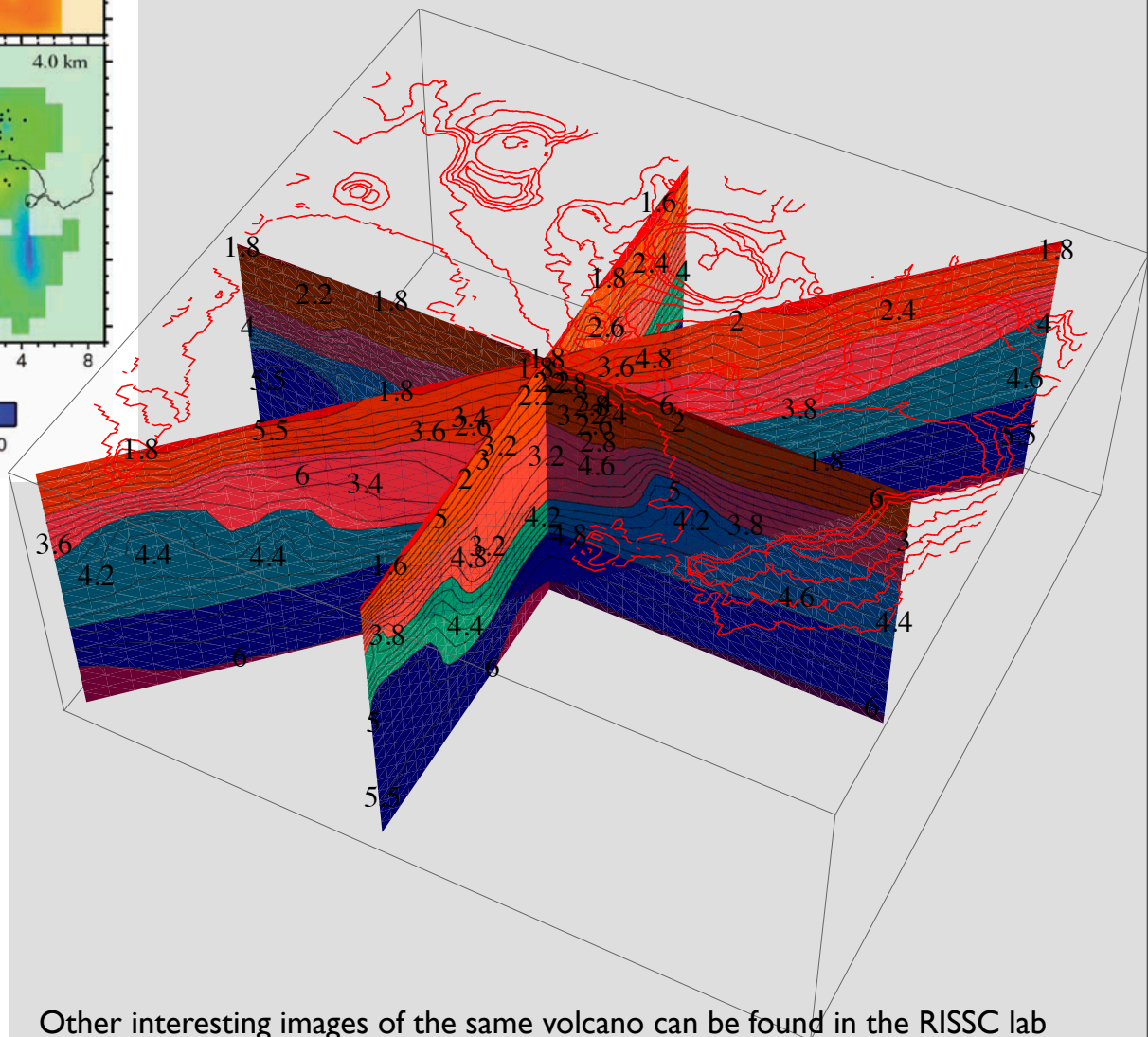

Other interesting images of the same volcano can be found in the RISSC lab home page (University of Naples, INGV and AMRA, (G. Iannaccone and A. Zollo coordinators) http://www.rissclab.unina.it/. The main projects are: Spice and DPC-INGV "UNREST"

Complementary information is given by attenuation images

Why attenuation images?

Pros

1 - major sensitivity to the presence of molten rocks

2 - easy to apply to shear waves

3 - add complementary information to the ordinary travel time tomography

4 - a linear inversion scheme

Cons

1 - major difficulty in the estimate of the seismic attributes

2 - biases introduced by the site effects

3 - the "total attenuation" is the sum of intrinsic and scattering attenuation coefficients, that are not separable in a single-path estimate.

Passive seismological methods to study the earth structure through attenuation tomography.

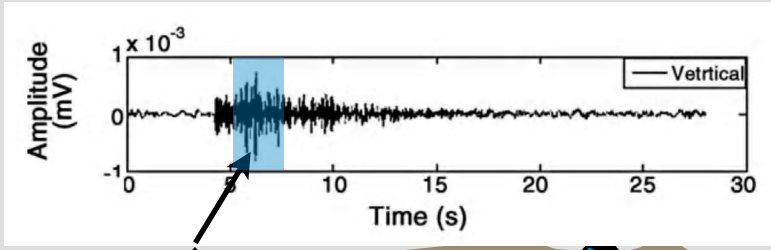

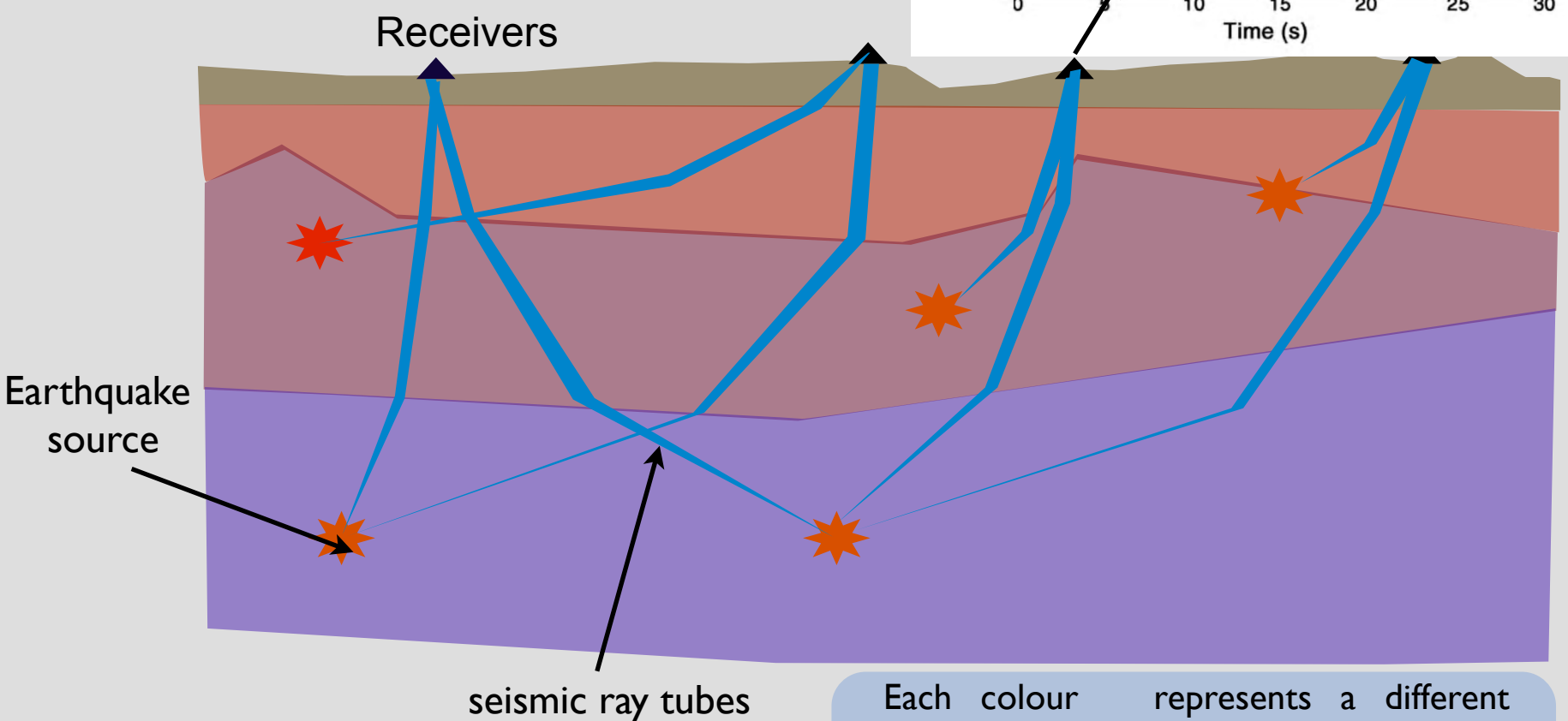

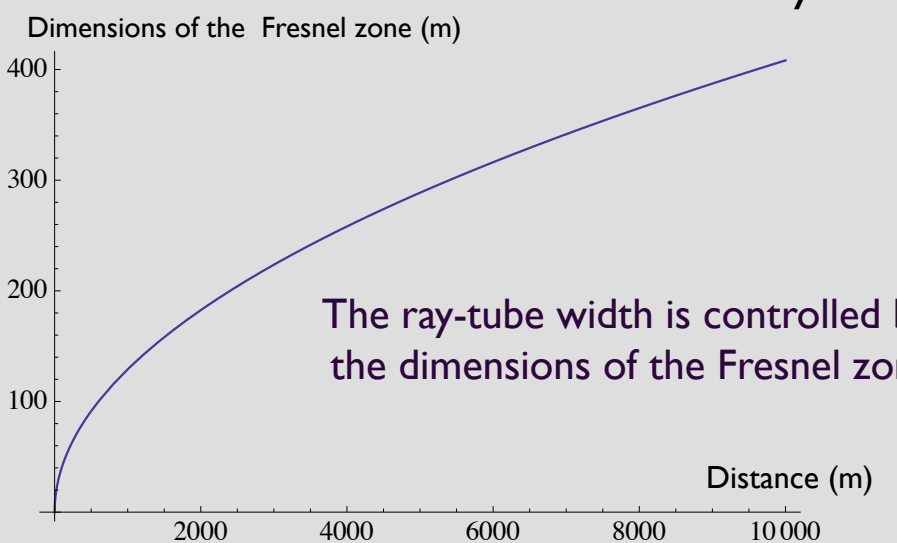

The ray-tube width is controlled by the dimensions of the Fresnel zone

Each colour represents a different lithology characterized by seismic velocity and attenuation coefficient. The attenuation tomography is based on a well known seismic velocity structure. Rays (Fermat principle) can be thus traced in the (known) velocity structure.
Differently from the active tomography, we cannot directly measure the energy (or intensity) decay along the path as we do not know the intensity at the source.

S- (and P-) waves energy spectrum

The high-frequency energy density for S (and P) waves can be expressed as the product of source (i), path (ij), site (j) and instrument effects (j) as:

$$E_{ij}(f,r) = S_i(f)\theta_{ij}(\vartheta,\phi)I_j(f)T_j(f)G_{ij}(r)\exp\left[-2\pi f\int_{\text{ray}}\frac{\mathrm{d}l}{v(l)Q(l)}\right]$$

$S_i(f)$ =*Source function*

$\theta_{ij}(\vartheta,\phi)$ =*Source radiation pattern*

$G_{ij}(r)$ =*Geometrical spreading term*

$I_j(f)$ =*Instrument transfer function*

$T_j(f)$ =*Site transfer function*

$Q_{\mathrm{T}}^{ij}(r)$ =*Total quality factor*

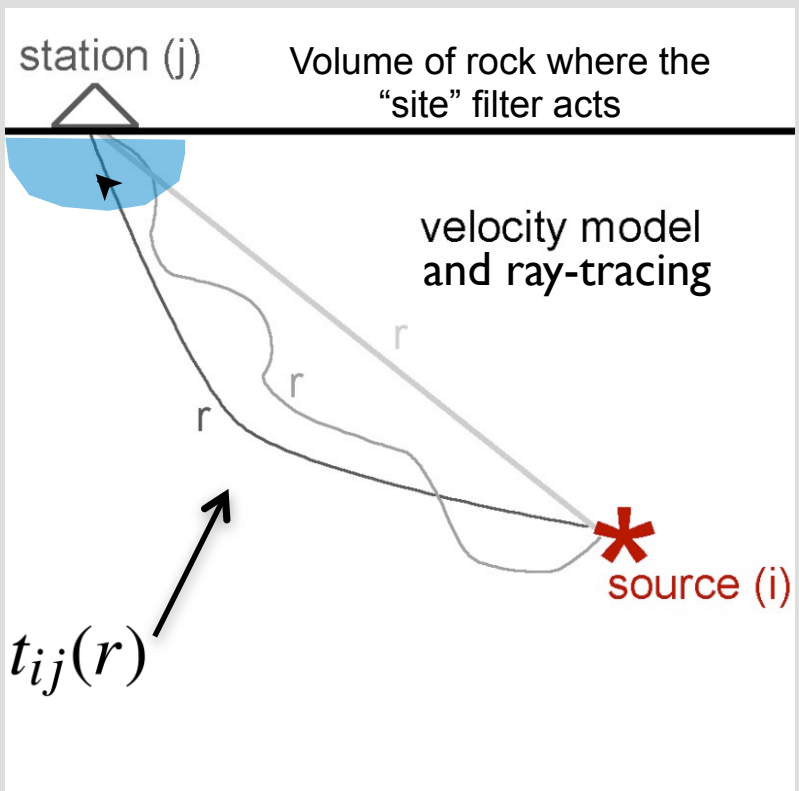

The only way to proceed is to assume the source spectral shape , and to measure the variation of the source spectral shape caused by the attenuation along the path.
Even tough the assumption about the spectral shape is well founded - the physics of the earthquake source is sufficiently known - there is further uncertainty for the presence of a “site” filter, that is in principle unknown. So, there is an unique way to overcome the problem: measure the site transfer function.

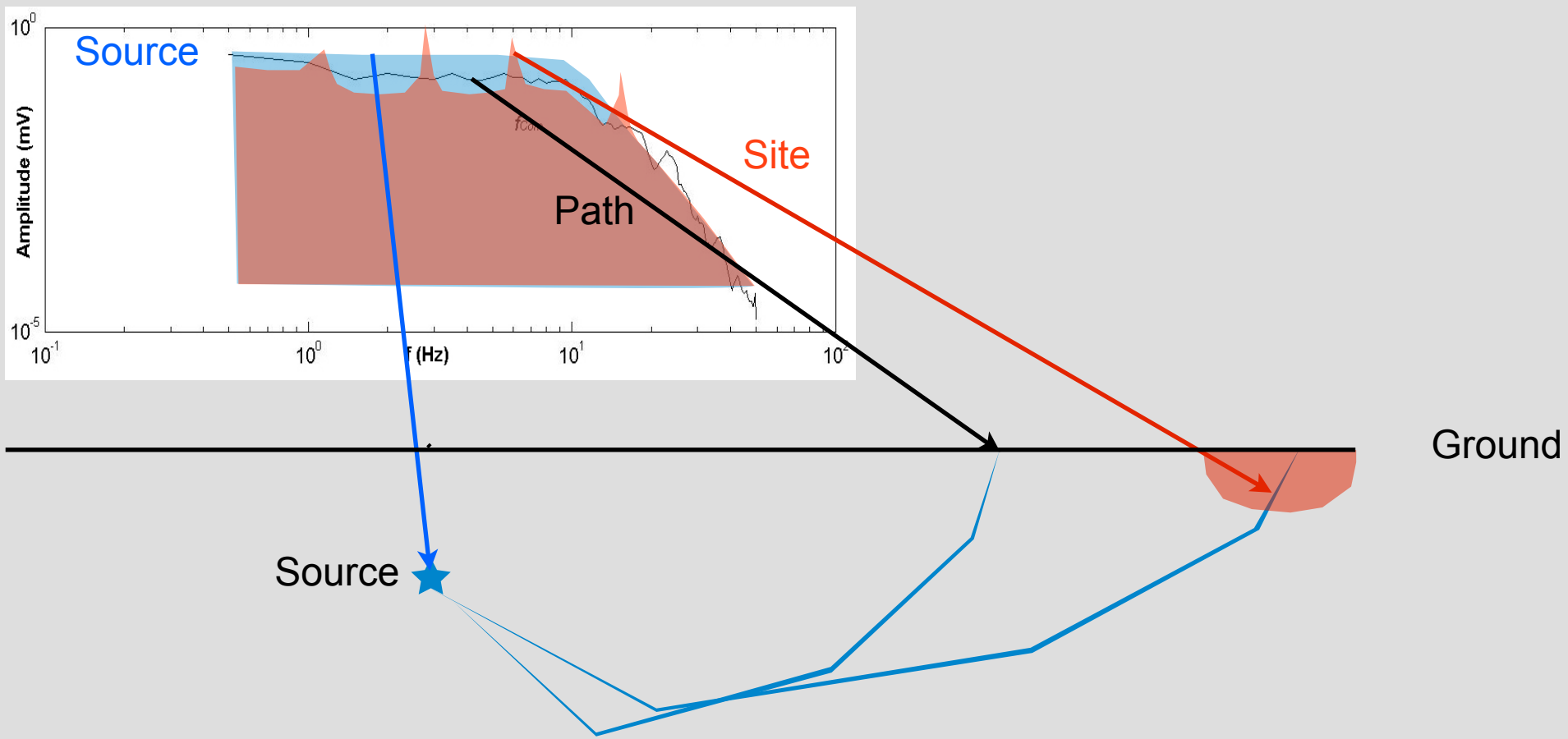

Generation of coda waves.

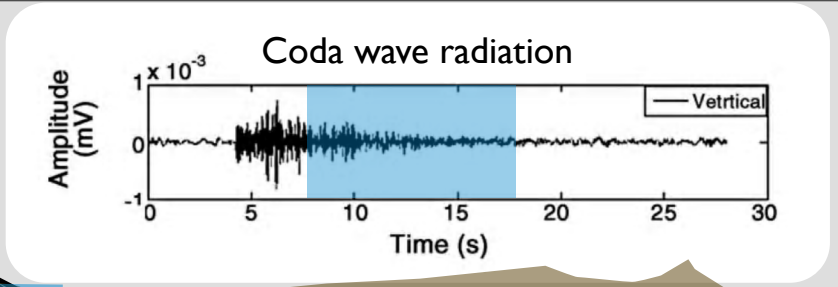

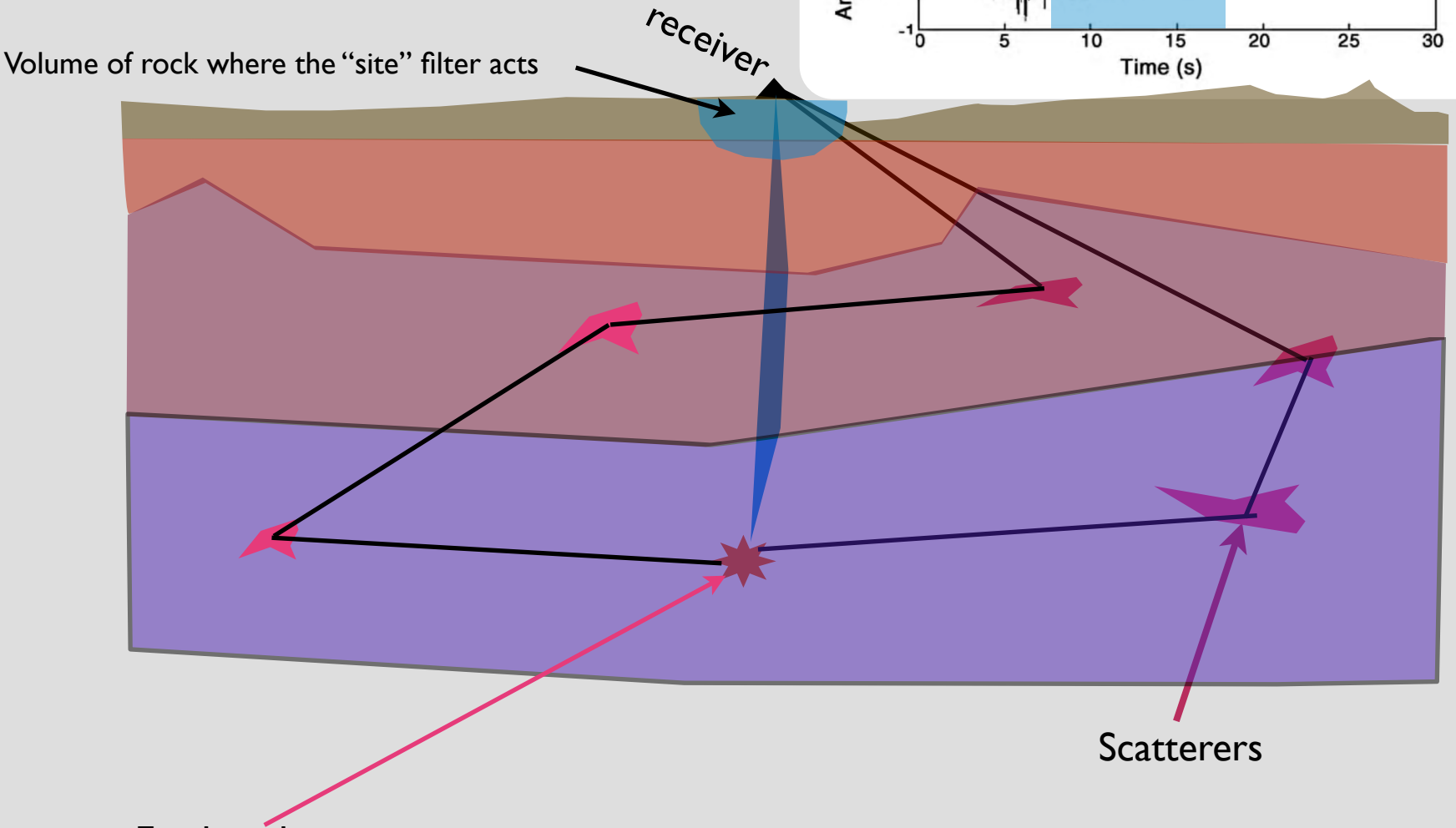

Scatterers are randomly distributed but homogeneously re-emit the primary energy as secondary waves in a scattering process forming the coda waves. The energy is summed up incoherently as the phase information is lost in the random process. In the coda the effects of Radiation pattern at source are space averaged. Both primary and secondary radiation are affected by site in the same way.

Coda waves spectral properties

- The coda wave spectral energy in the interval around the lapse time tc, can be expressed as the product of source, path, site and instrument effects as:

$$E^C(f, t_c) = S_i(f) I_j(f) T_j(f) P(f, t_c)$$

- At any lapse time (t_c) measured from the origin time, the coda source intensity, instrument and site functions equal those for S-waves.
- Coda waves are not affected by radiation pattern effects.
- The propagation term is dependent of the average coda spectrum, characteristic of the area

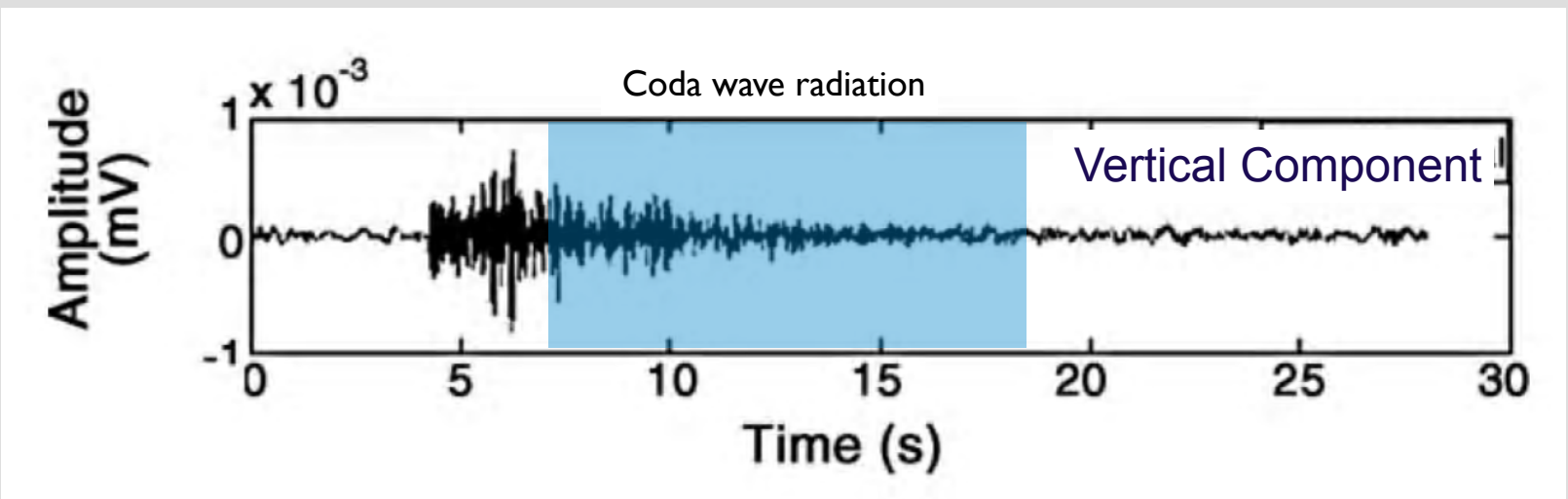

Normalization for the site transfer function using coda wave properties

- High frequency seismograms show the effect of scattering of high frequency P- and S-wave radiation by the medium heterogeneity in the coda.
- Coda is the wave train following the direct S-wave radiation
- Due to the very nature of the coda waves, generated by the sum of incoherent radiation coming from any direction, the source radiation pattern effects are averaged out in the coda.
- Site effects affect in the same way both the coda wave spectrum and the S-wave spectrum

Registrations of a VT quake at short distance with a three component seismic station

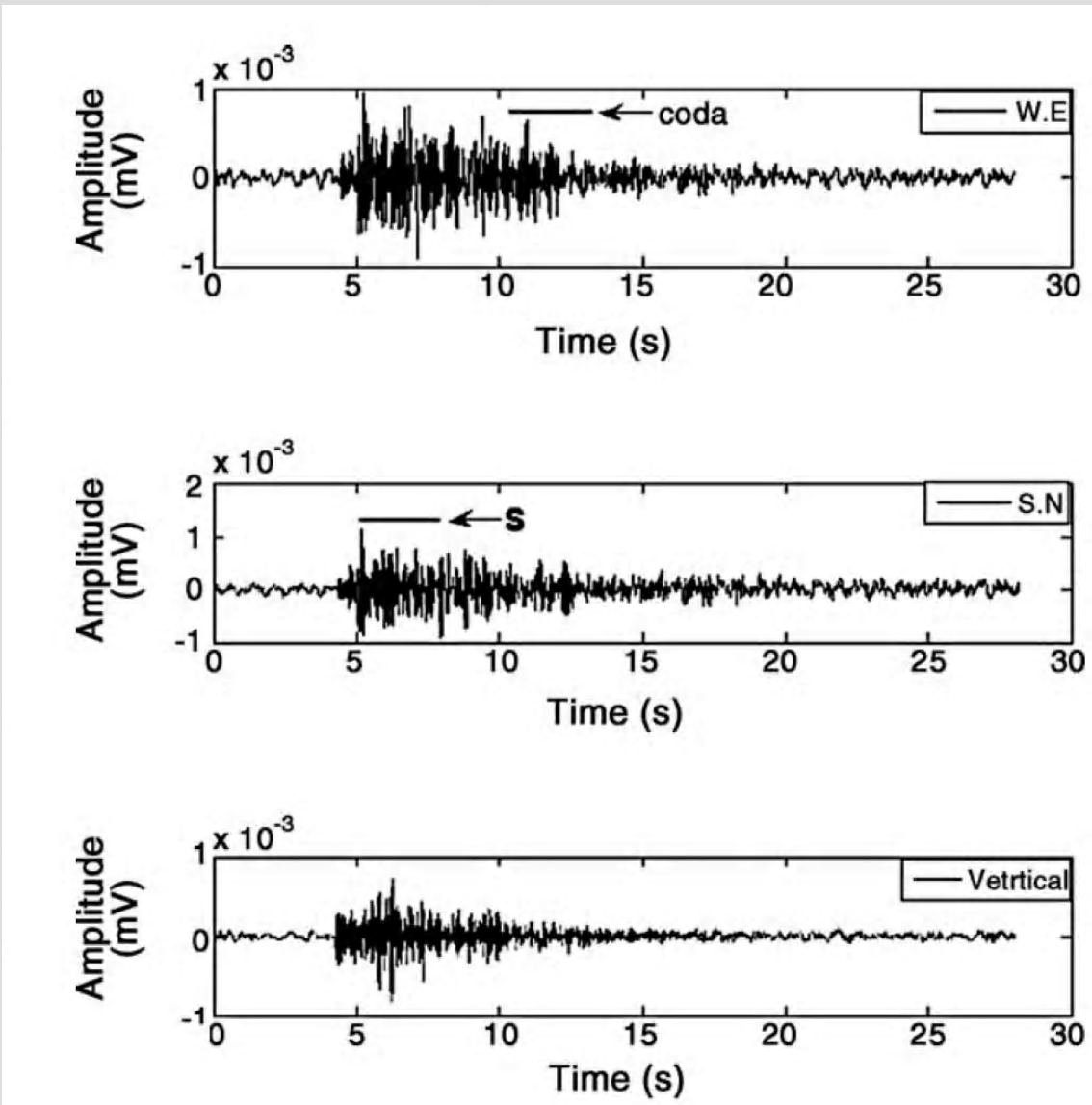

In the early coda source radiation pattern is averaged

Can I find a window length for S-waves for which the effect of the radiation pattern is no more present, like in coda waves?

Immediately after the S waves onset the so called "early coda" begins. The effect of the radiation pattern decreases for increasing window length.

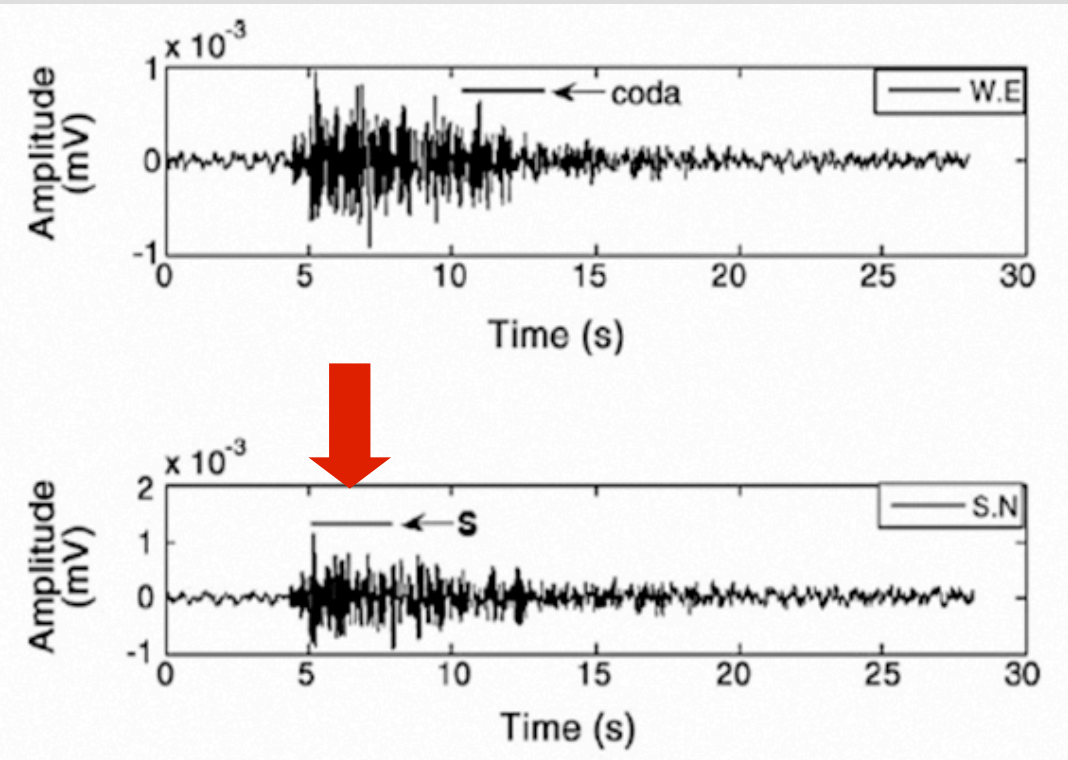

Experimental observations on early coda

• The rms of the S-wave radiation, in the interval between t_S and t^*, is calculated at the receivers for a single seismic event. This quantity fluctuates mainly due to radiation pattern effects; its standard deviation, σ, measures these effects.
• Increasing t^*, σ decreases.
• An evident "change point" has been experimentally found using a statistical test.

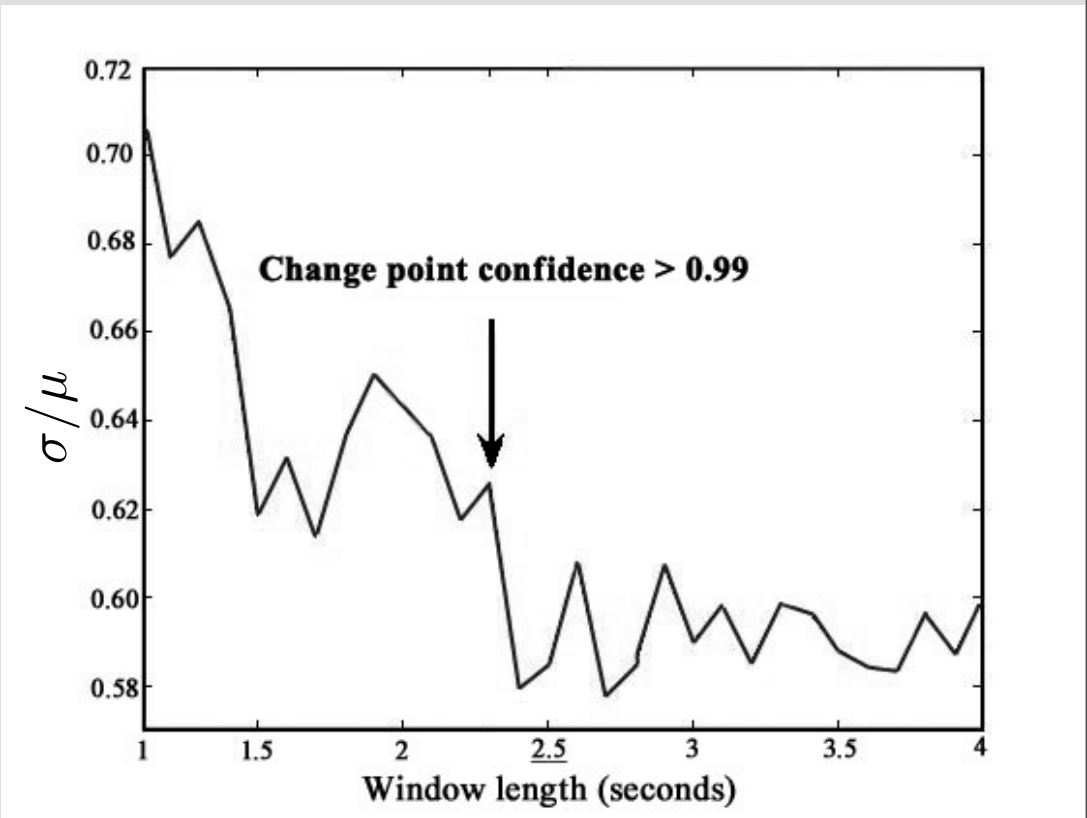

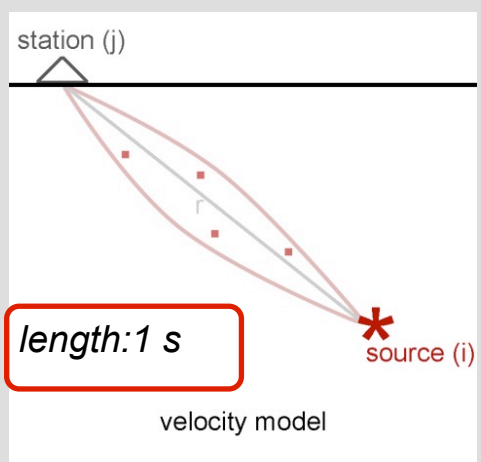

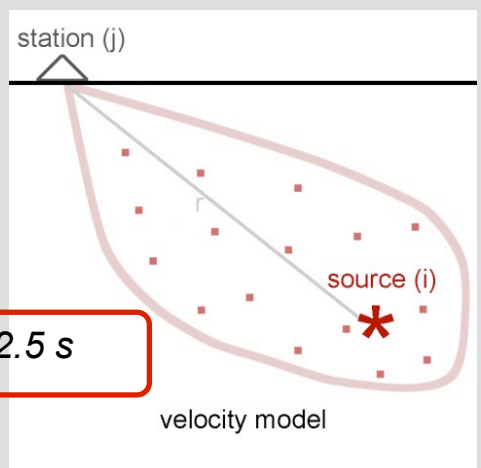

A time window of 2.5 seconds averages the effect of radiation pattern!

The Coda-Normalization (CN) method

- Normalizing the S-waves energy with the coda waves energy:

$$\frac{E_{ij}(f,r)}{E^{C}(f,t_c)} = \frac{\theta_{ij}(\vartheta,\phi)}{P(f,t_c)} G_{ij}(r)\,\exp\left[-2\pi f \int_{\text{ray}} \frac{\mathrm{d}l}{v(l)Q(l)}\right]$$

- Assuming $\theta_{ij}(\vartheta,\phi)$ = const and $G_{ij}(r)=r_0^2/r^2$ the remaining unknown is the S waves quality factor.
- It results experimentally that $P(f,t_c)$ = const.
- Substituting energy with amplitude and taking the logarithm:

$$\ln\left(\frac{|A_{ij}^{S}(f)|}{|A_{ij}^{C}(f,t_c)|}\cdot r_{ij}\right) = K(f,t_c) - \pi f \int_{r_{ij}} \frac{\mathrm{d}l}{v(l)Q(l)}$$

Discretizing the problem

$$R_{ij} = K(f) - \pi f \sum_{b=1}^{B} l_{ijb} s_b Q_b^{-1}$$

The inverse problem

- The earth structure under study is parametrized using a cubic grid of side=a.
- The velocity model is known at a detail greater than the grid side a.
- The inversion problem can be rewritten:

$$R_{ij} = K(f) - \pi f \sum_{b=1}^{B} l_{ijb} s_b Q_b^{-1}$$

$$C(f) - \frac{R_k}{\pi f} = \sum_{b=1}^{N\_cells} l_{kb} s_b Q_b^{-1}$$

$$\mathbf{d}(f) = \mathbf{G}\mathbf{m}(f)$$

$$R_{ij} = \ln\left(\frac{|A_{ij}^{S}(f)|}{|A_{ij}^{C}(f, t_c)|} \cdot r_{ij}\right)$$

B =total number of blocks

l_{ijb}=length of the segment in block b

s_b =slowness of block b

Hereafter I will refer to the k-th ray

Modified slope decay (SD) method

The S- (or P-) waves spectrum can be written:

$$A_{\mathrm{ij}}{}^{\mathrm{HF}}[f,r] = S^{A}{}_{i}[f] I_j[f] T_j[f] G_{\mathrm{ij}}[r] \exp\left[-\pi \mathrm{f} \int_{\mathrm{ray}} \frac{s(l) r(l)}{Q(l)} dl\right]$$

$$S_i^A[f] = \frac{\Omega_0}{\left[1 + \left(\frac{f}{f_{\mathrm{Corn}}}\right)^{\gamma \mathrm{n}}\right]^{\frac{1}{\gamma}}}; n = 2; \gamma = 2$$

$$T_j[f] = T'[f] \exp[-\pi \mathrm{kf}]$$

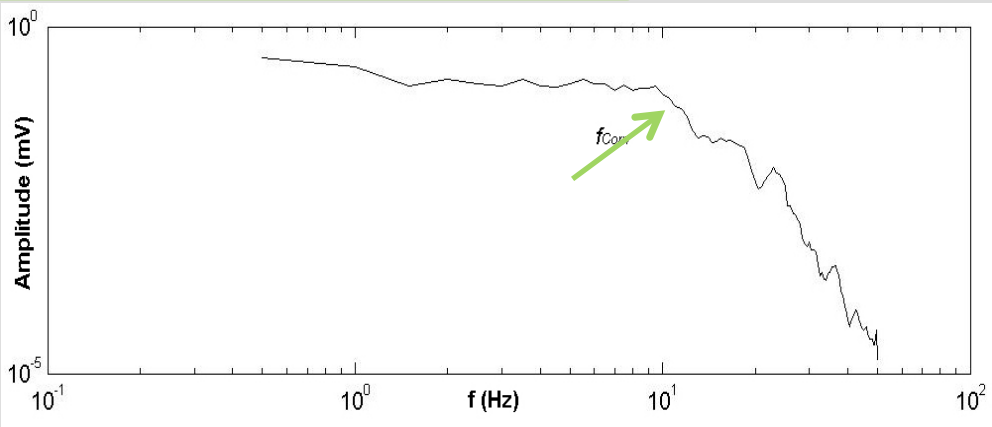

taking the frequency derivative of the log:

$$\frac{\partial}{\partial f}\left[\ln\left[A_{\mathrm{ij}}{}^{\mathrm{HF}}\right]\right] = -2\frac{f^3}{{f_{\mathrm{Corn}}}^4 + f^4} - \pi \mathrm{k} + \frac{\partial}{\partial f}\left[\ln\left[T'_{\mathrm{ij}}\right]\right] - \pi \int_{\mathrm{ray}} \frac{s(l) r(l)}{Q(l)} dl$$

$$d_m^D = \frac{1}{\pi}\left[-\frac{\partial}{\partial f}\left[\ln\left[A_m{}^{\mathrm{HF}}\right]\right] - 2\frac{f^3}{{f_{\mathrm{Corn}}}^4 + f^4} - \pi \mathrm{k} + \frac{\partial}{\partial f}\left[\ln\left[T'_j\right]\right]\right.$$

$$\tilde{d_m^D} = \sum_{b=1}^{\mathrm{N\_cells}} l_{\mathrm{mb}} s_b Q_b^{-1}$$

As evident, both methods to obtain the seismic attributes lead to the same formulation of the inverse problem. Moreover, assuming

$$Q_b^{-1} = < Q^{-1} > + \delta Q_b^{-1}$$

We obtain

$$\widehat{d_m^D} = \sum_{b=1}^{\mathrm{N\_cells}} l_{\mathrm{mb}} s_b < Q^{-1} > + \sum_{b=1}^{\mathrm{N\_cells}} l_{\mathrm{mb}} s_b \delta Q_b^{-1}$$

Or, shifting in the left hand side the coefficients

$$\overline{\overline{d_m^D}} = \sum_{b=1}^{\mathrm{N\_cells}} l_{\mathrm{mb}} s_b \delta Q_b^{-1}$$

Implicitly we assume that attenuation changes δQ_b^{-1}

are small as compared with $< Q^{-1} >$

Solving the overdetermined equation system

$$d = G \cdot m \;\rightarrow\; m = \left(G^T G\right)^{-1} G^T d$$

It may happen that the condition number of the matrix to be inverted is not small. In practice this means that rays do not homogeneously sample the earth volume under study. This makes the optimization problem mixed-determined.

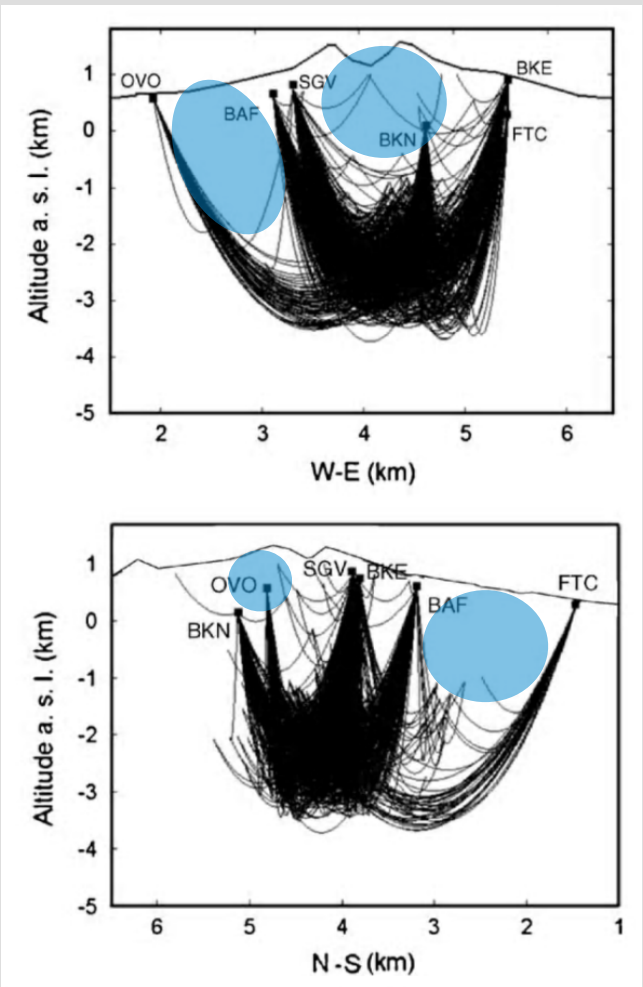

Consequently, the matrix can be partitioned through SVD, a damped (l.s.) solution, or some "a-priori" information can be used (Menke, pag.55-59)

In the applications, we used some a-priori information to "force" the cubic cells where no (or few) rays pass through at the value of $< Q^{-1} >$. Inversion in both areas has been carried out using a multi-step approach.

Multi-resolution inversion

It is well known that the resolution of seismic imaging depends both on the wavelength (which should be smaller than the cell size) and the number of rays sampling the single cell [*Bai and Greenhalgh*, 2005].

In the present dataset, a frequency of 6 *Hz* corresponds to a wavelength of about 250 m for S-waves and of about 500 m for P-waves. For the same data, the average Fresnel radius, which is calculated for the average ray length of 3:2 km, is less than 400 m for S-waves and less than 500 m for P-waves.

Consequently, we assume a minimum cell size of 500 m. This is the cell size associated with the zones of maximum ray coverage. Outside this zone, a cell with a 1000 m size is assumed.

We first invert for a structure of 1000 m cell size, and then constrain the zones with maximum resolution (there are eight 500 m side cells in a single 1000 m side cell!) to have as average the Q measured in the 1000 m side cell.

Mt. Vesuvius multi scale attenuation

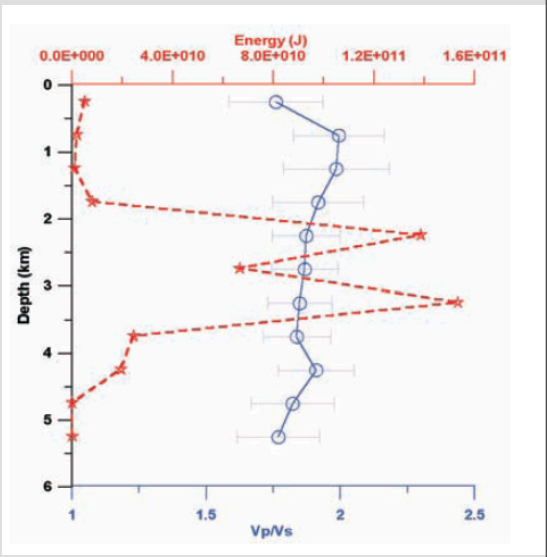

data - set
826 VT earthquake
7 stations
2203 rays

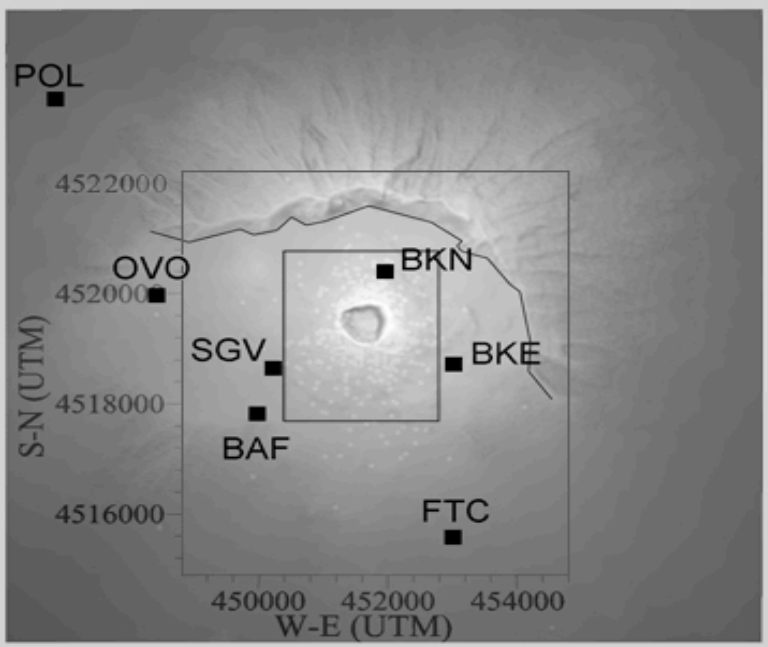

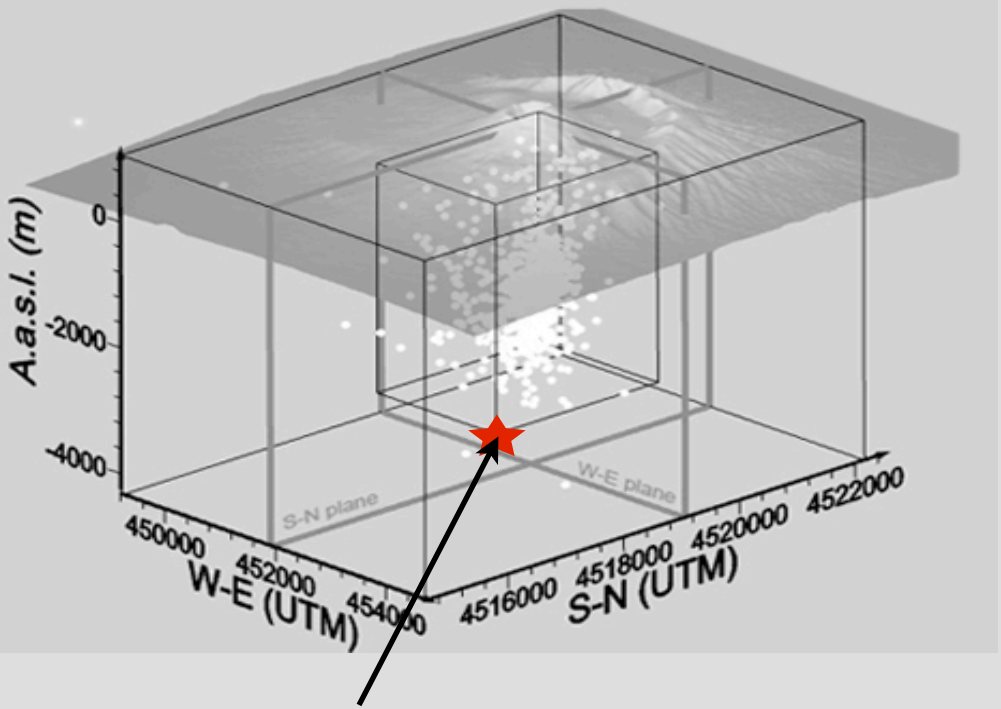

Max Magnitude = 3.6
Inner Volume: Max resolution zone
Ray-tracing: Thurber-modified approach

Checkerboard tests

Checkerboard test in the High-Resolution volume

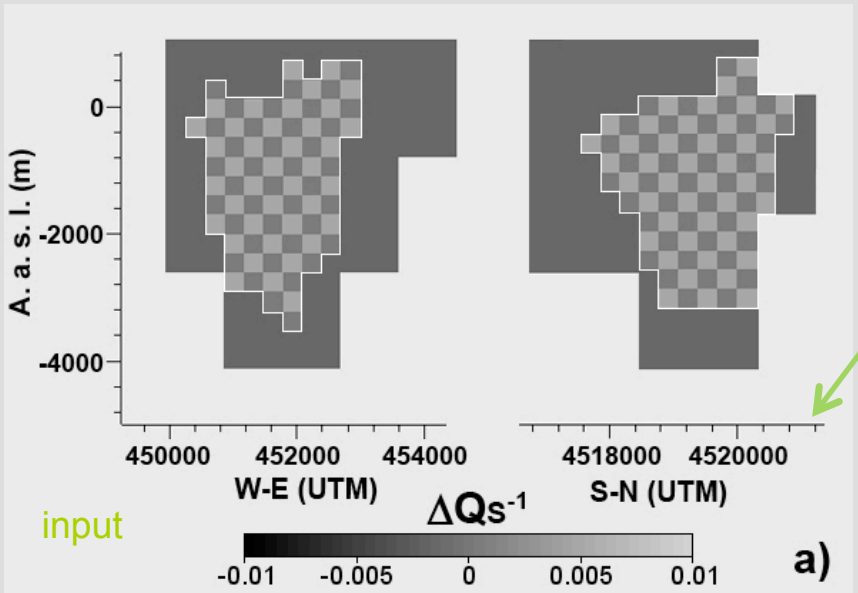

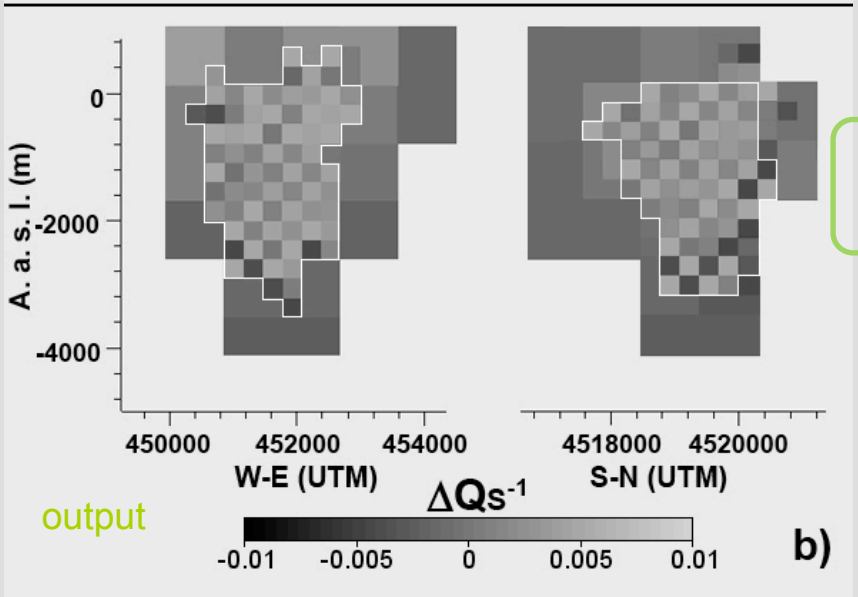

vertical cross-sections

horizontal cross-sections

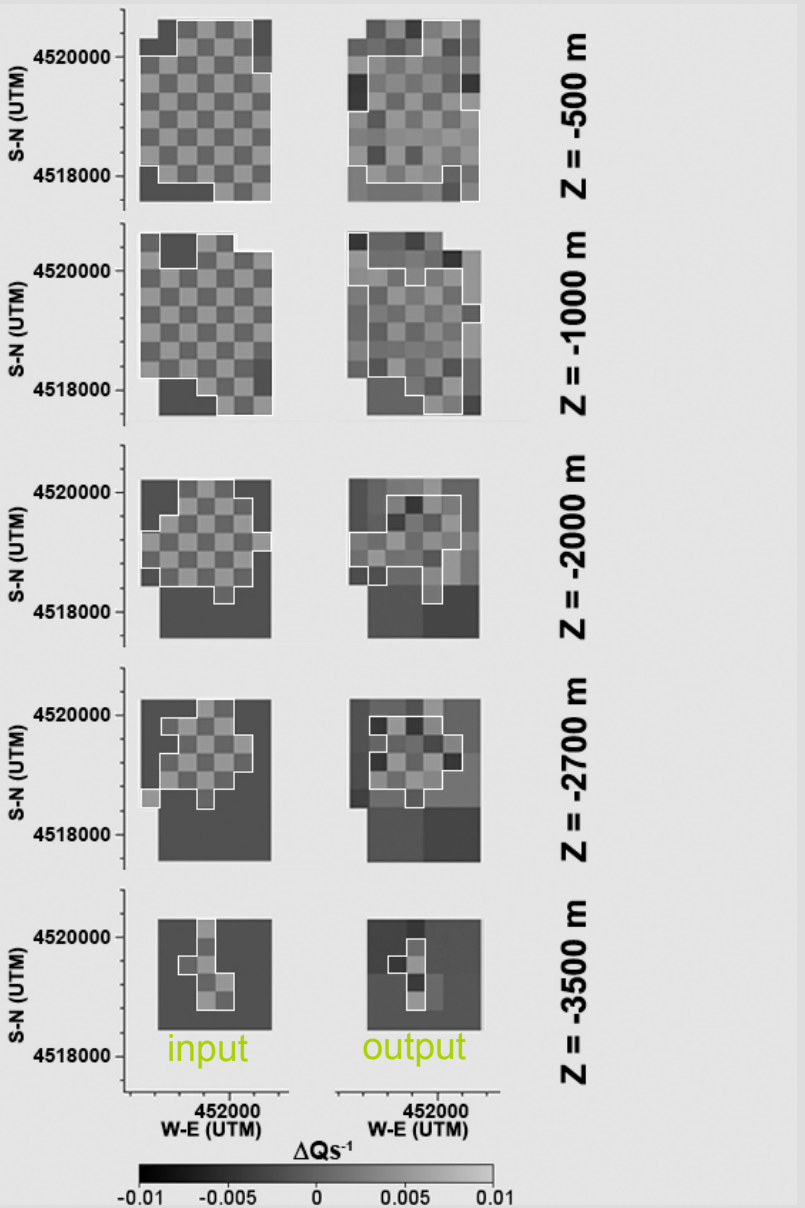

Robustness and stability tests

Robustness: what happens to the results when I randomly reduce my data-set?

• using a bootstrap approach, on average, I obtain robust estimates for a reduction of more than 40% of the data-set, for the blocks of 1800 m and 900 m side.

•the estimates for the blocks of 300 m side are robust for a reduction of more than 20% of the data-set.

Stability: what happens to the results when I change the constants in the inversion problem ?

•the constants are K(f) and the average Q of the area

•the results are not particularly affected by the variation of K(f)

•on average I obtain stable measures of attenuation for the blocks of 1800 and 900 side.

•the results at 300 m are affected by >40% changes of the average attenuation.

Resolution test

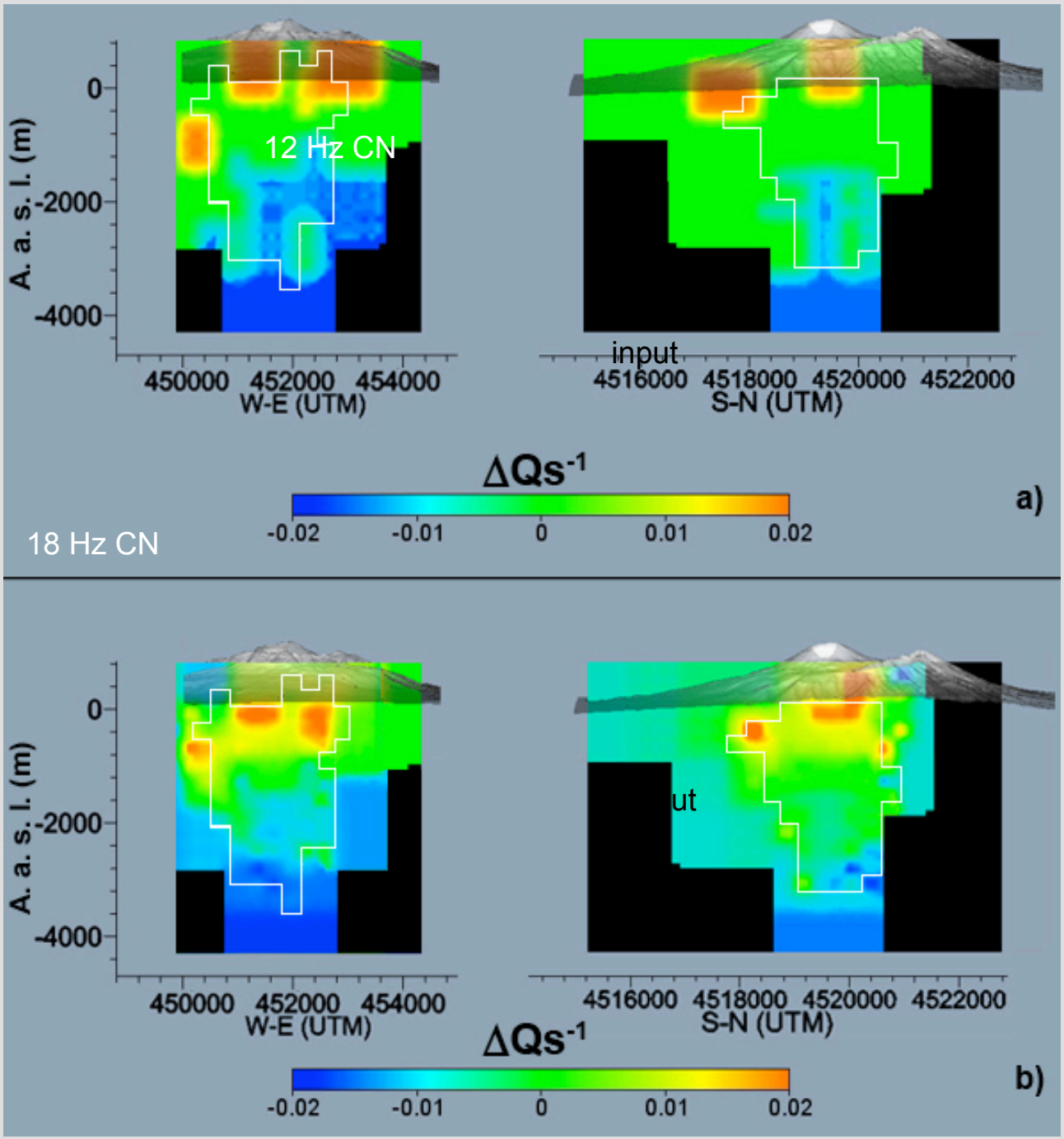

The synthetic anomaly test used to validate the results shows a good reconstruction of the anomalies in the high resolution region.

P-Velocity (left) and S-attenuation (right) images of Mt. Vesuvius

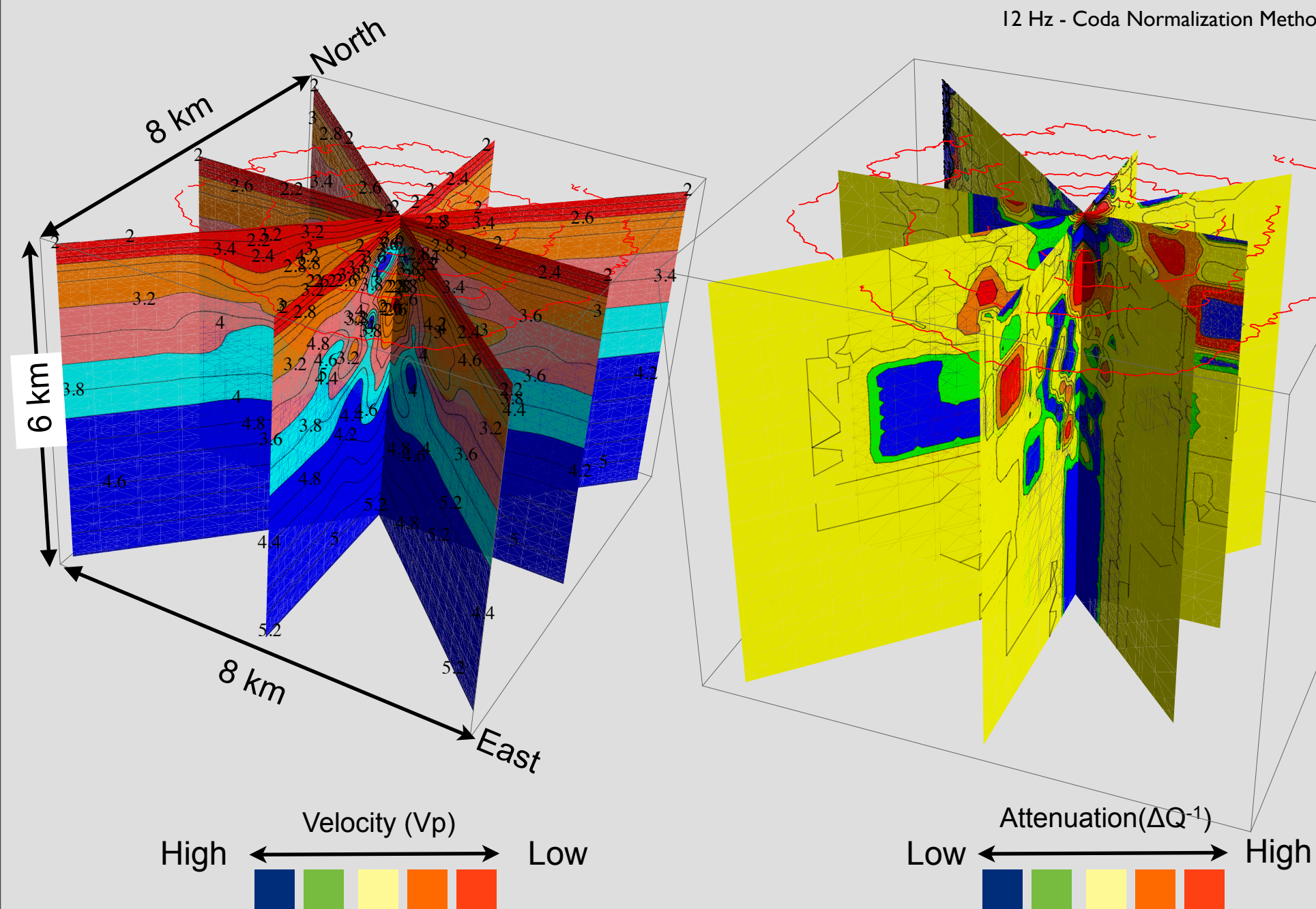

Mt. Vesuvius. Vertical sections S-N and W-E, intersecting at the crater axis

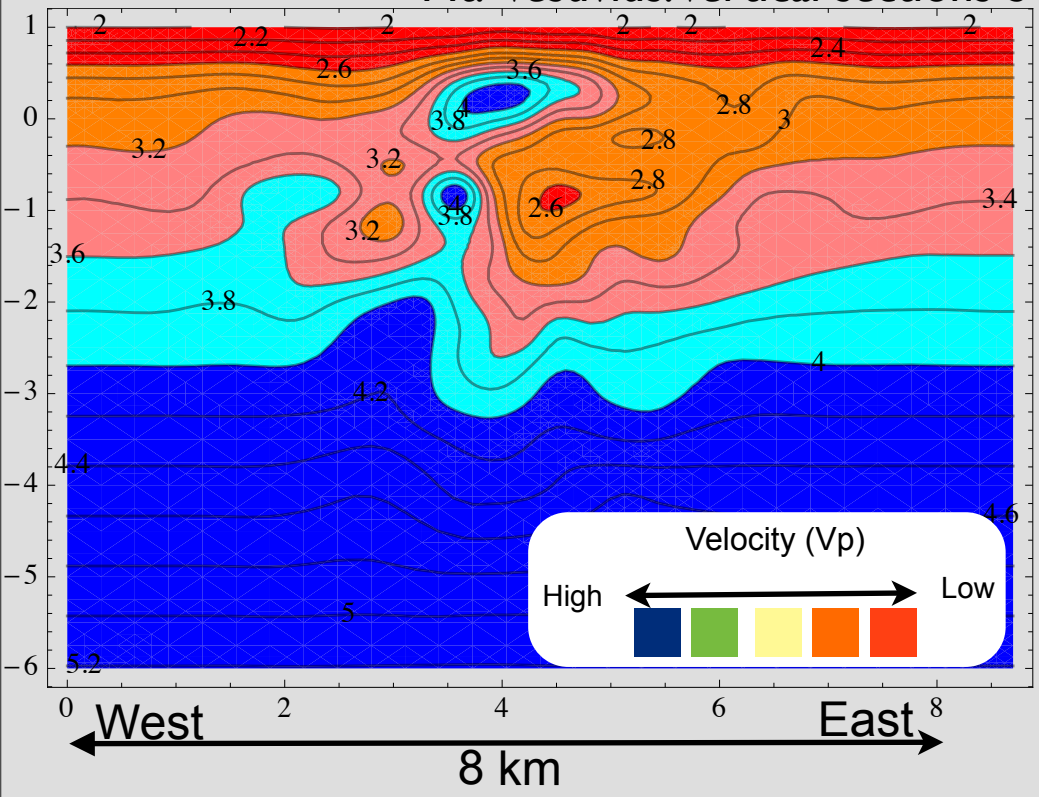

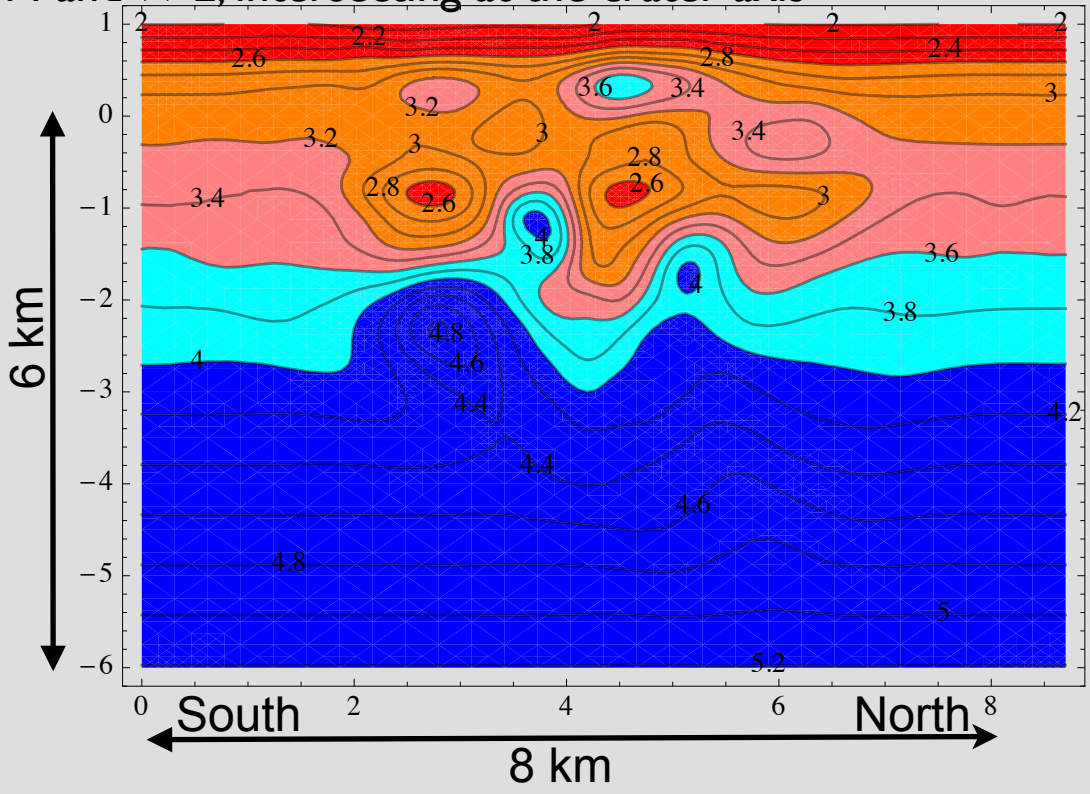

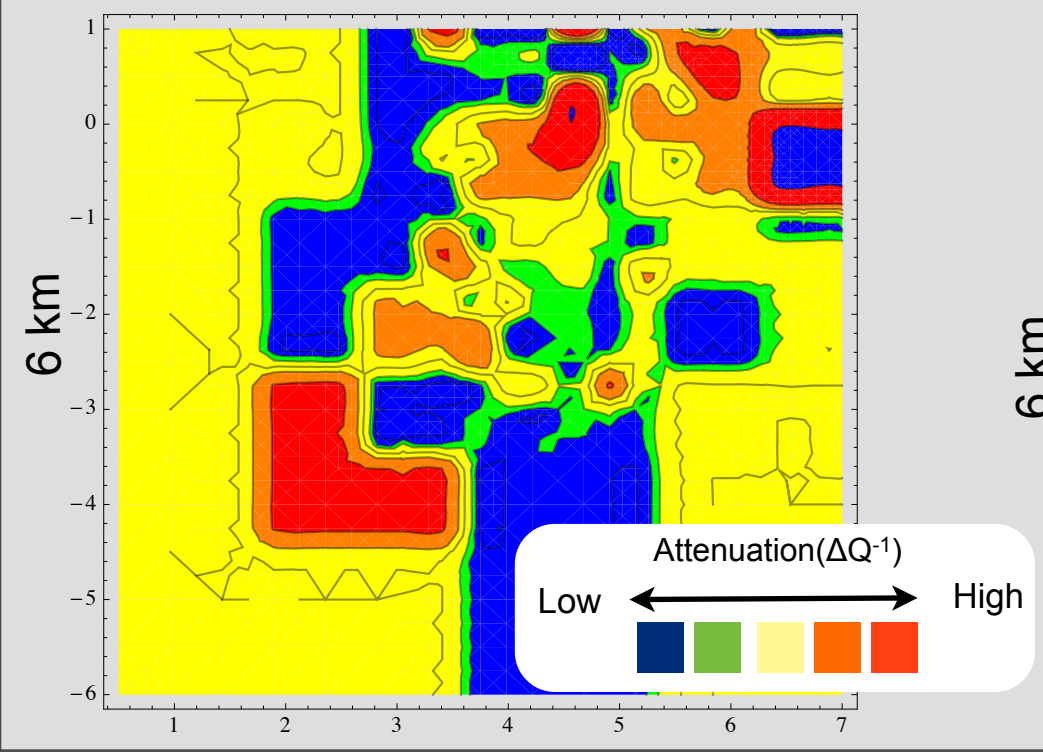

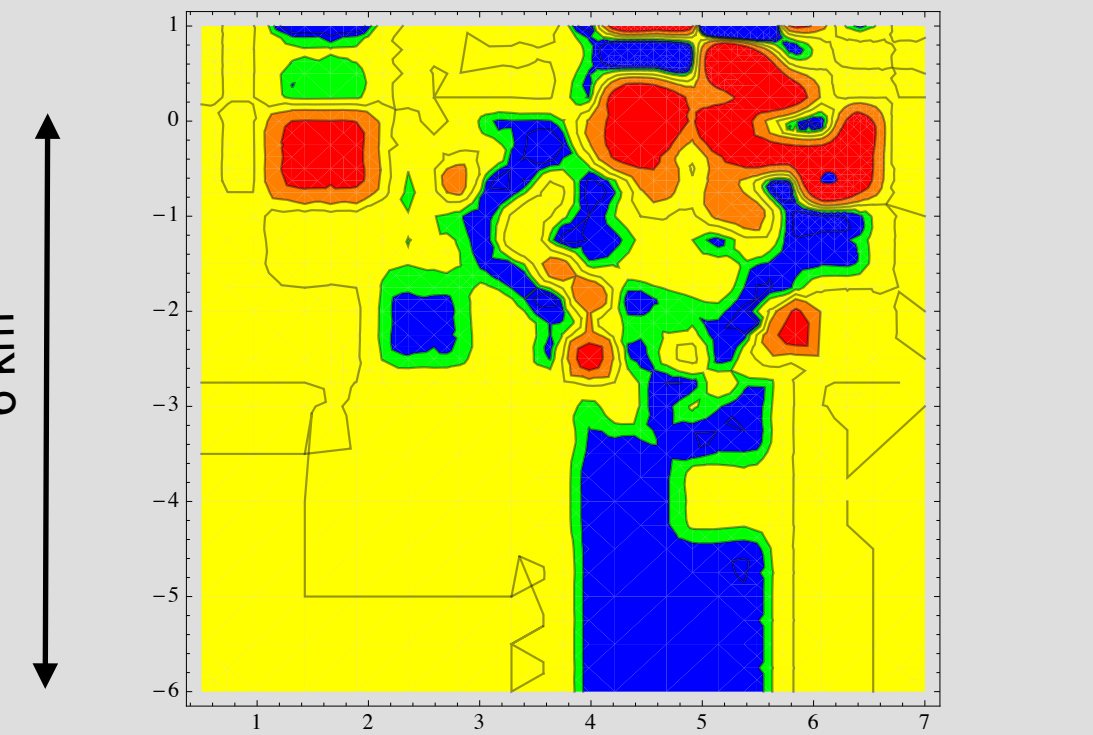

Mt. Vesuvius. Vertical sections S-N and W-E, intersecting at the crater axis

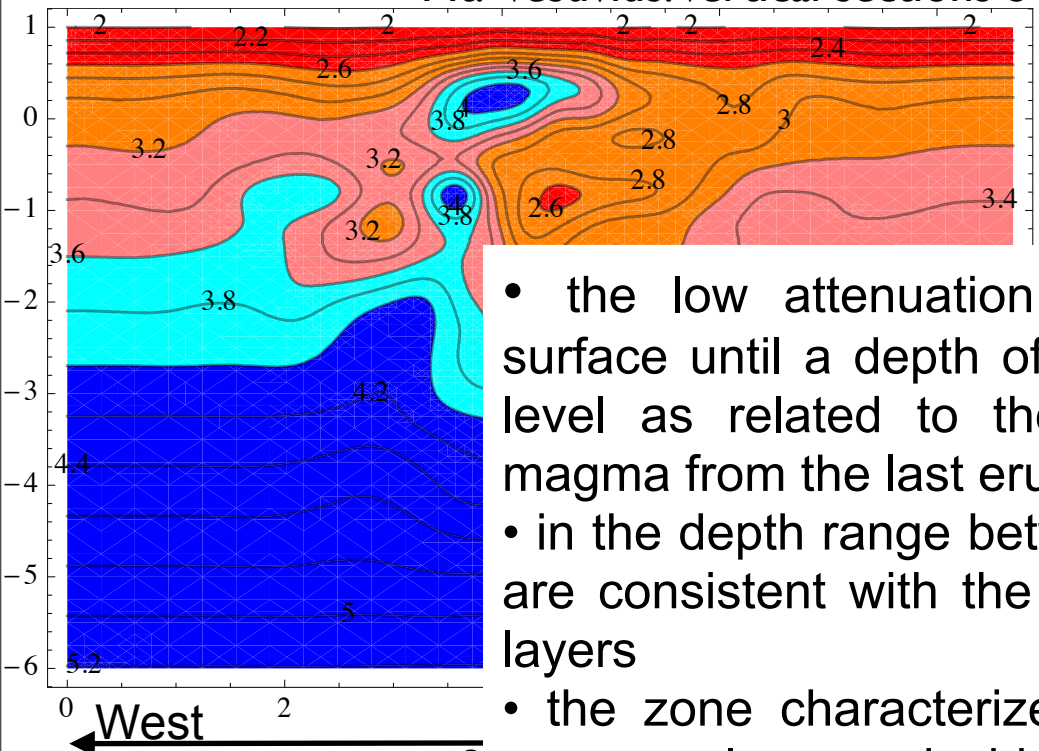

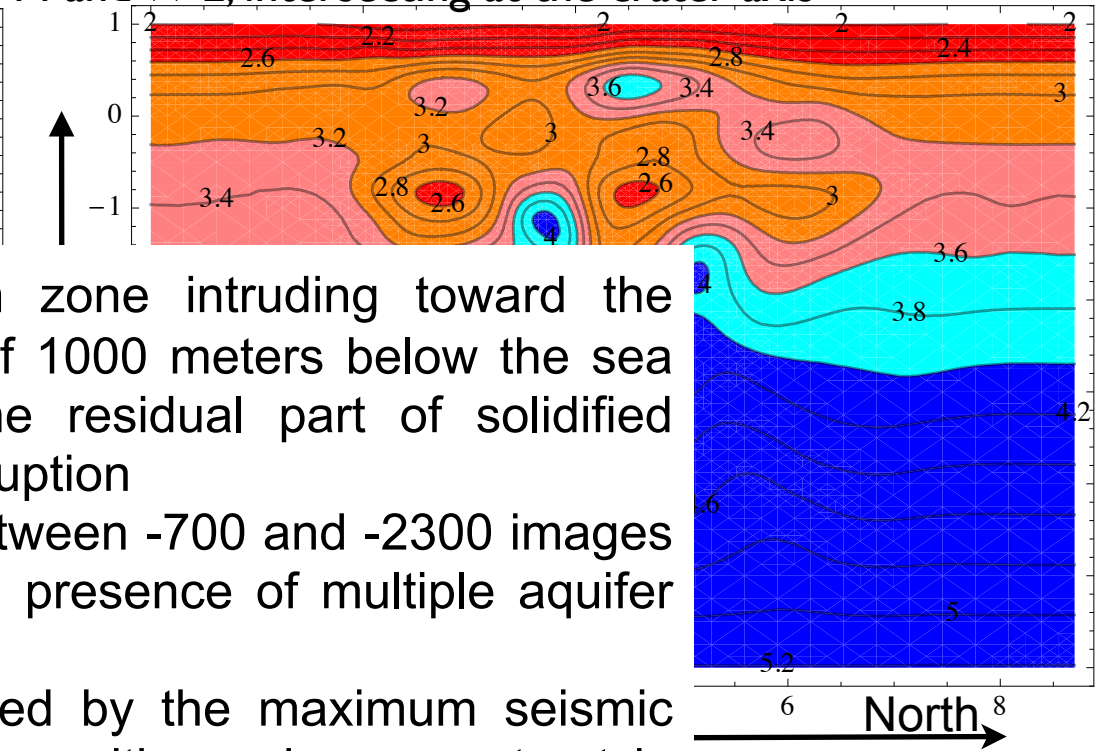

- the low attenuation zone intruding toward the surface until a depth of 1000 meters below the sea level as related to the residual part of solidified magma from the last eruption
- in the depth range between -700 and -2300 images are consistent with the presence of multiple aquifer layers
- the zone characterized by the maximum seismic energy release coincides with maximum contrast in attenuation and velocity, interpreted as a cracked medium.

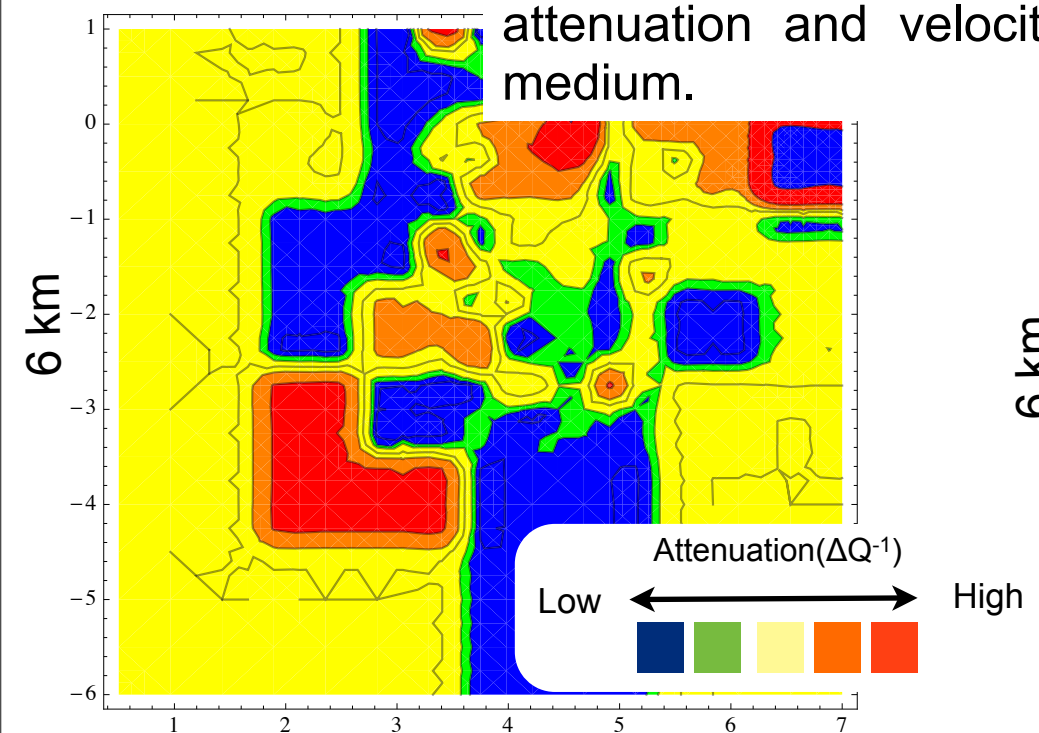

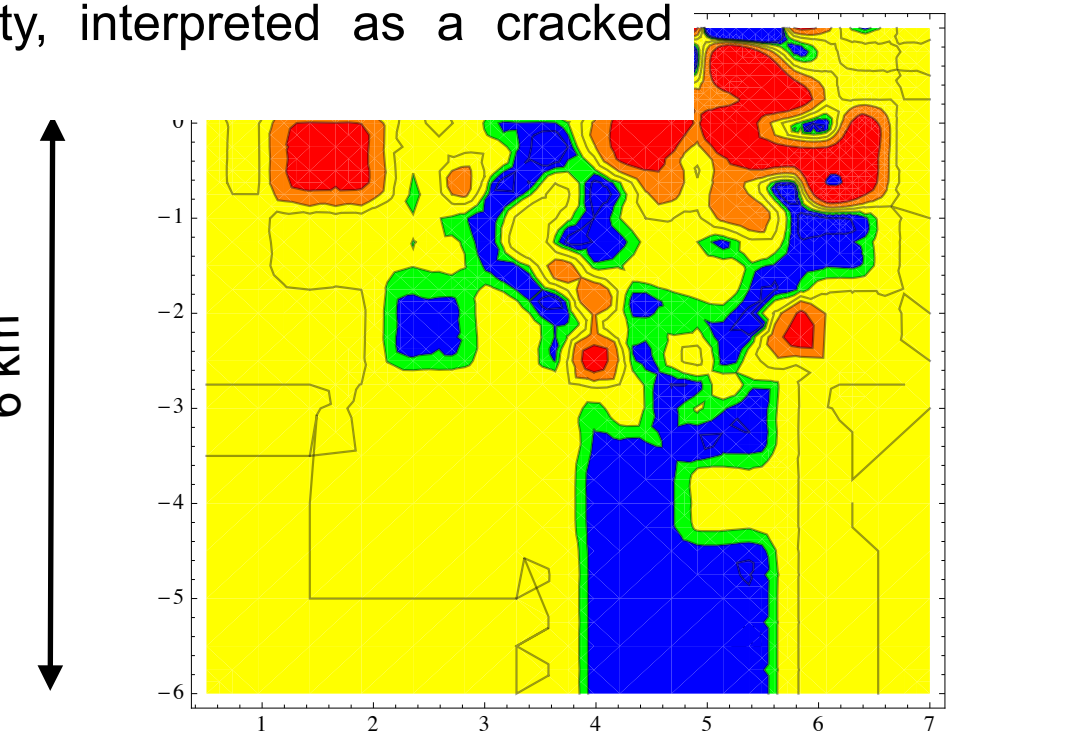

A qualitative scheme, to better summarize

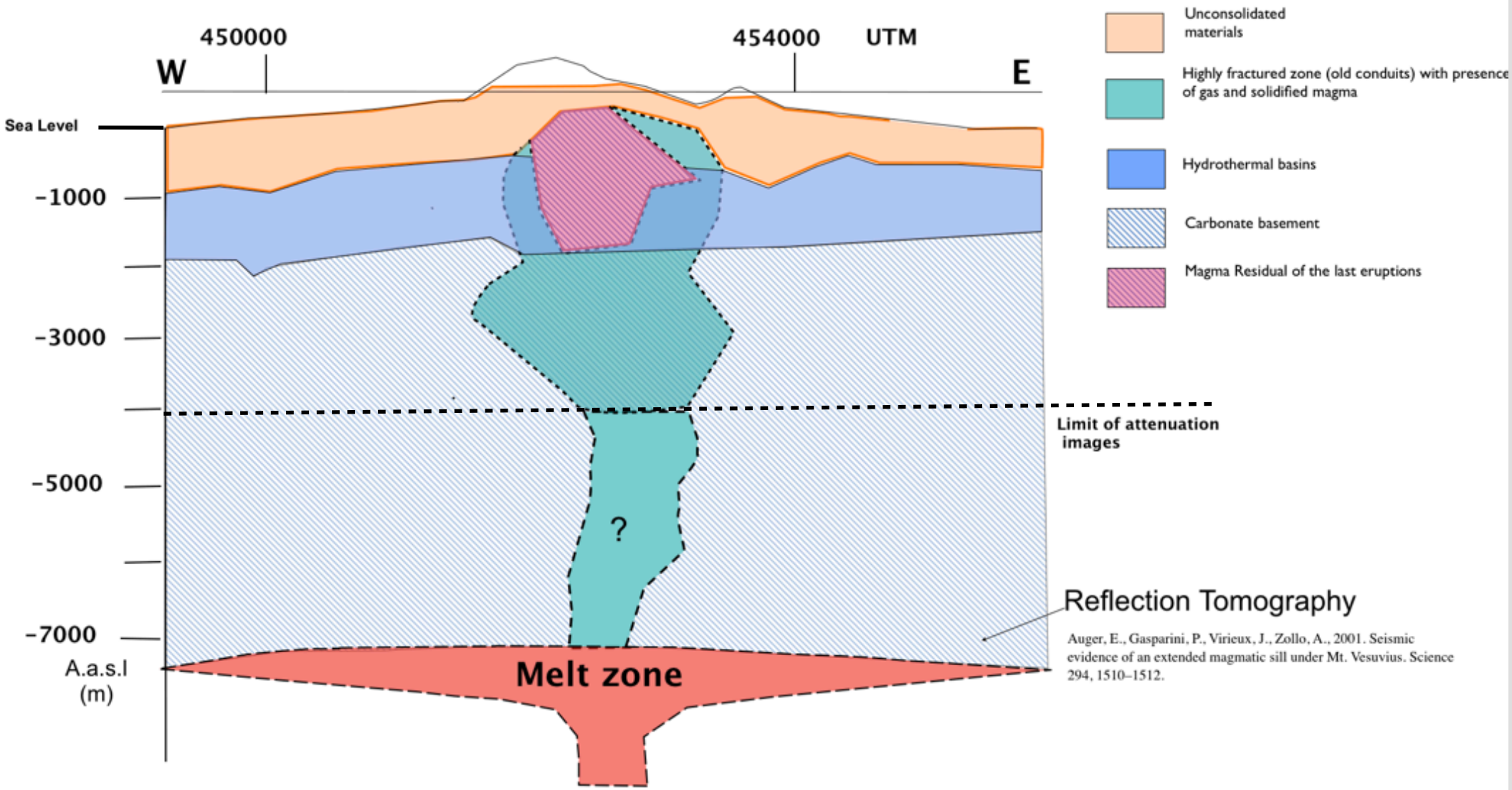

The area of Campi Flegrei, near Naples.

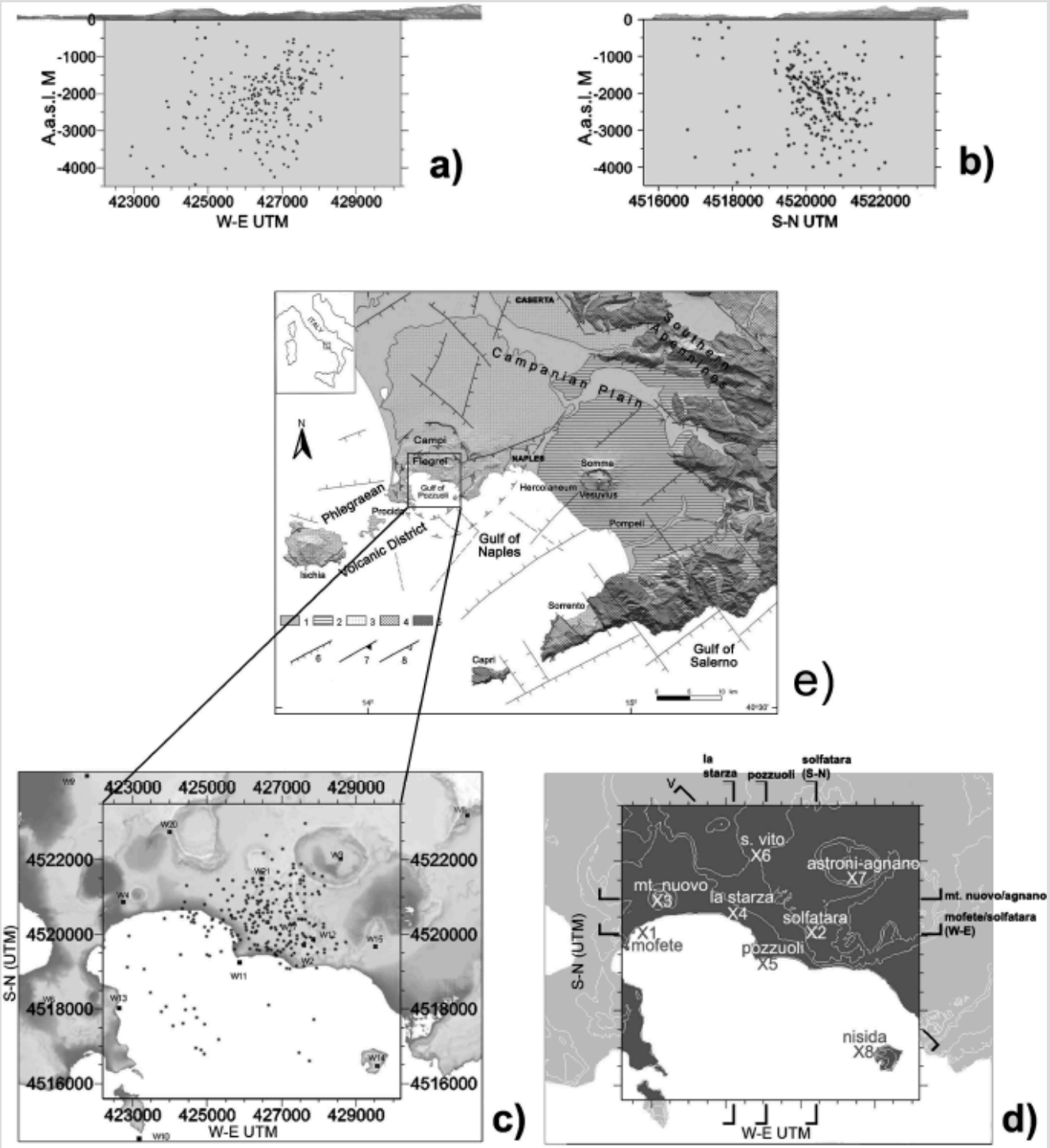

VT seismicity (1982 - 1984)
246 quakes recorded at 15
1-Hz digital stations

The bay of Naples, Vesuvius and Campi Flegrei.

The main volcanological features

Local seismicity is the input for tomography (passive).

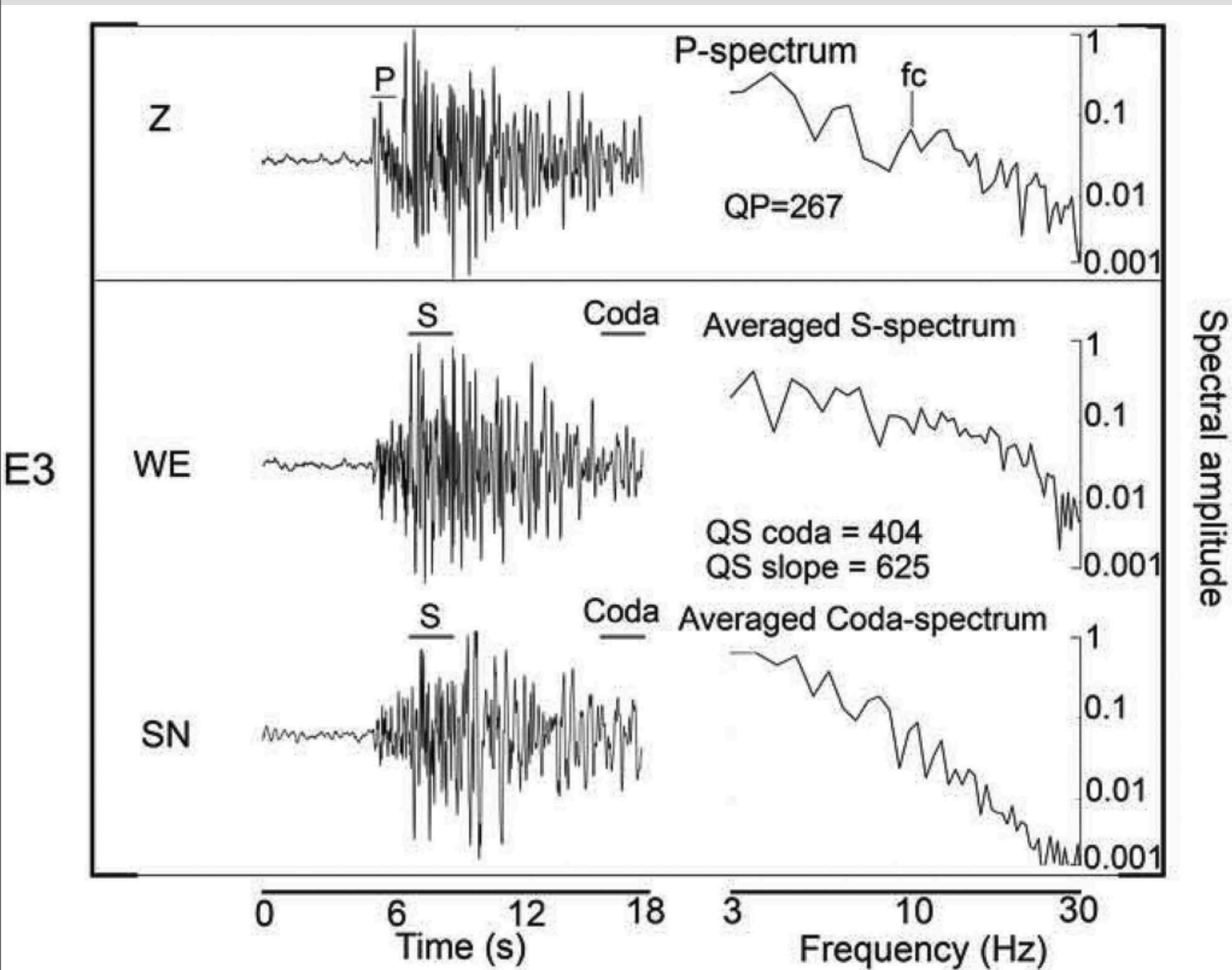

First column: the horizontal and vertical registrations of an example event. The origin time of each event is set to 0. the P-, S- and coda-windows used to measure spectra are indicated on each trace.
Second column: P- and averaged (on the two horizontal component) S- and coda-spectra; the corner frequency (fc) as well as the P- (*QP*) and S- wave (*QS CN*, *QS SD*) single path quality factors obtained with different methods are also indicated.

Tests similar to those for Vesuvius: spread function, checkerboard, synthetic anomaly. Dashed lines border the high-resolution volume. Left: S-waves. Right P-waves.

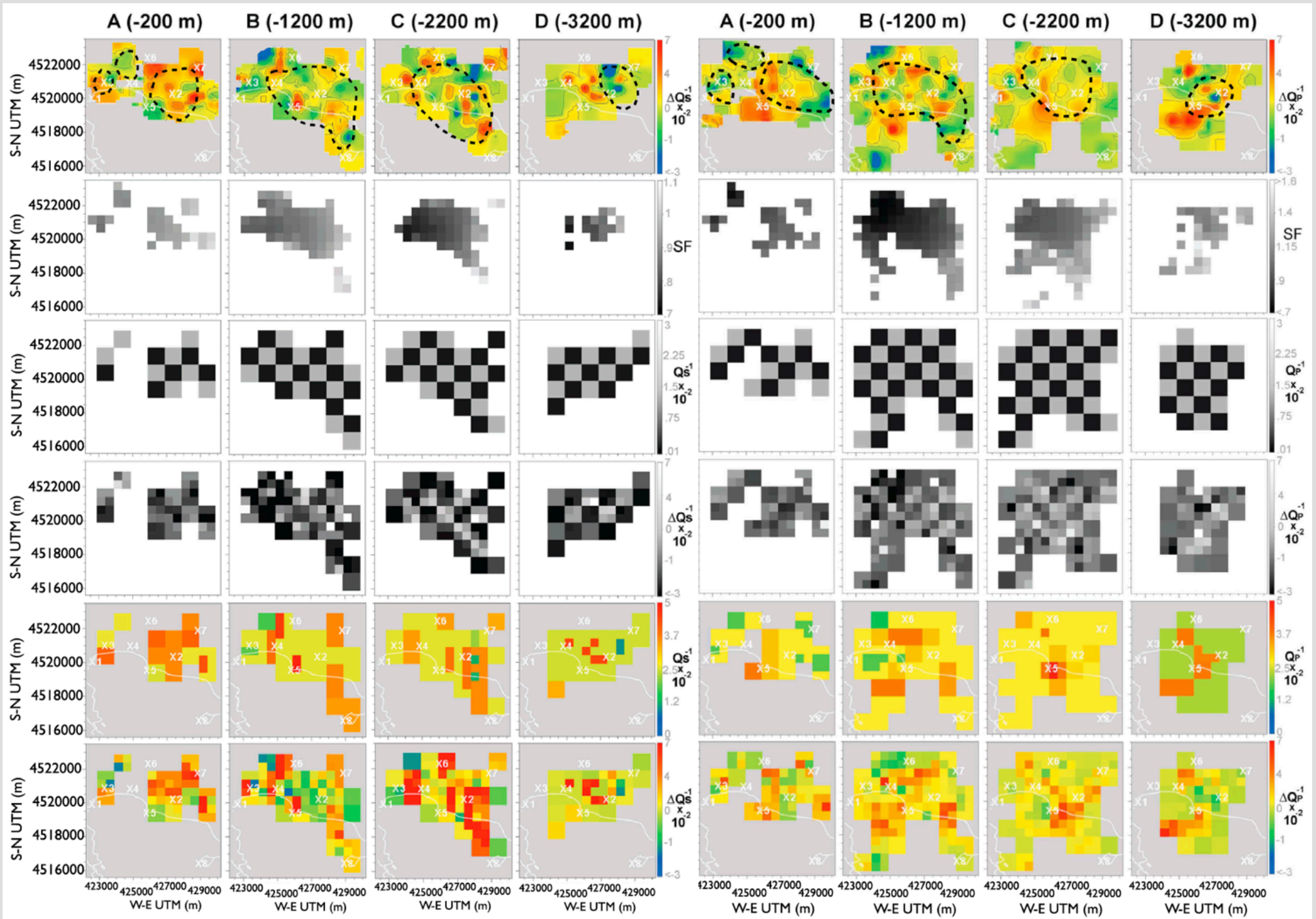

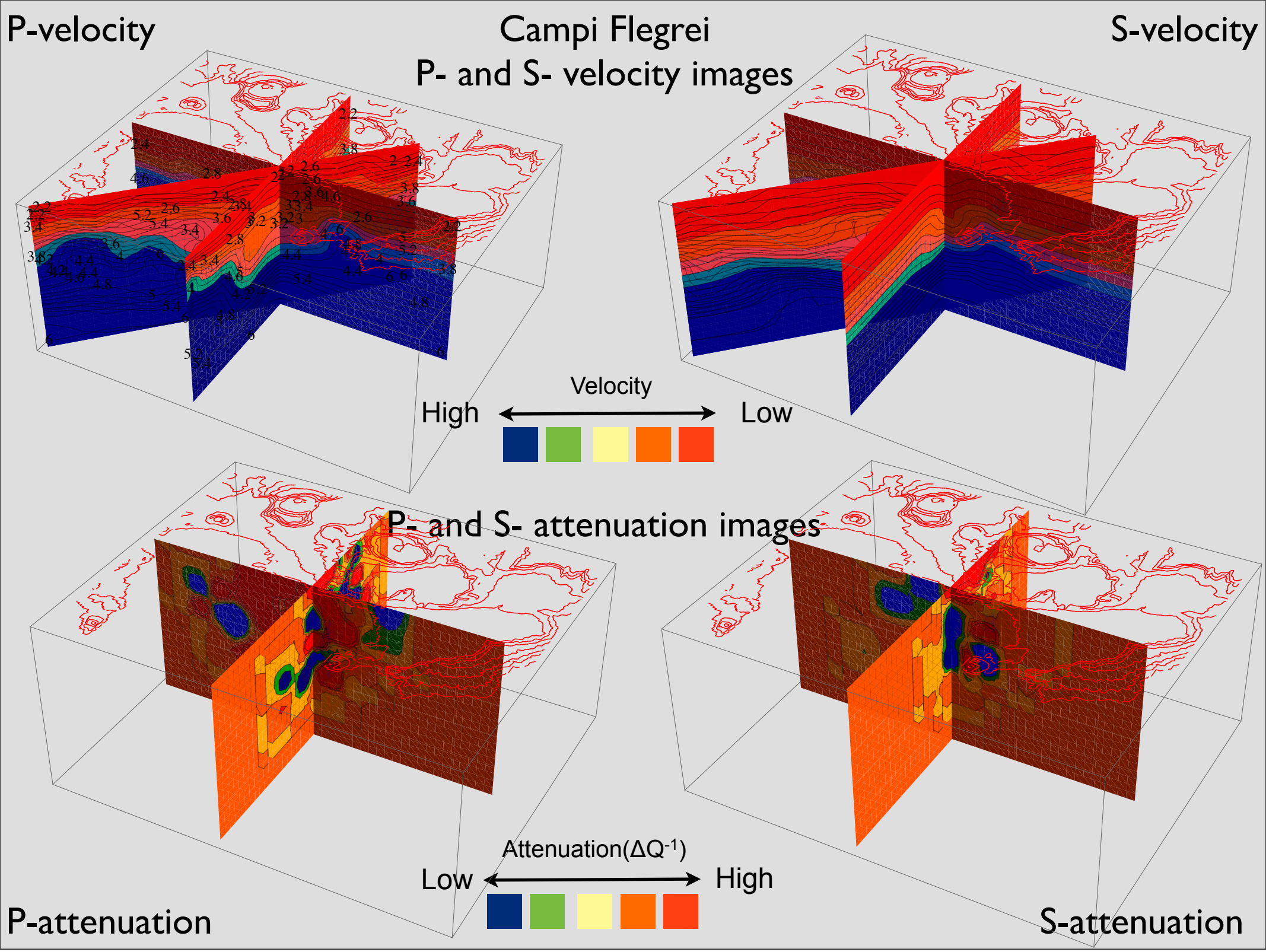
P-velocity
Campi Flegrei
P- and S- velocity images
S-velocity
Velocity
High
Low
P- and S- attenuation images
Attenuation(ΔQ-1)
Low
High
P-attenuation
S-attenuation

Campi Flegrei

Vertical sections S-N and W-E, intersecting the center map, P-waves

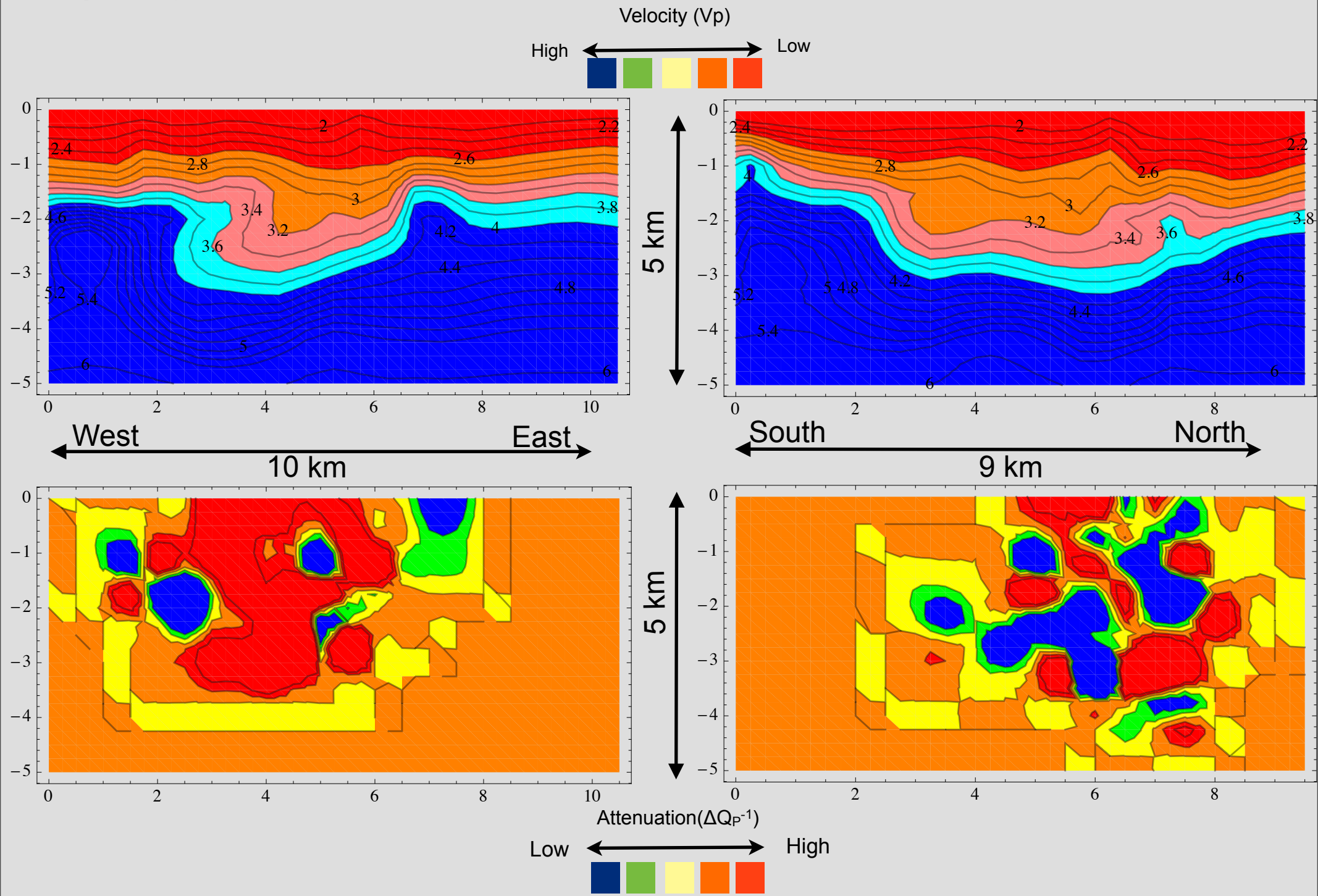

Campi Flegrei

Vertical sections S-N and W-E, intersecting the center map, S-waves

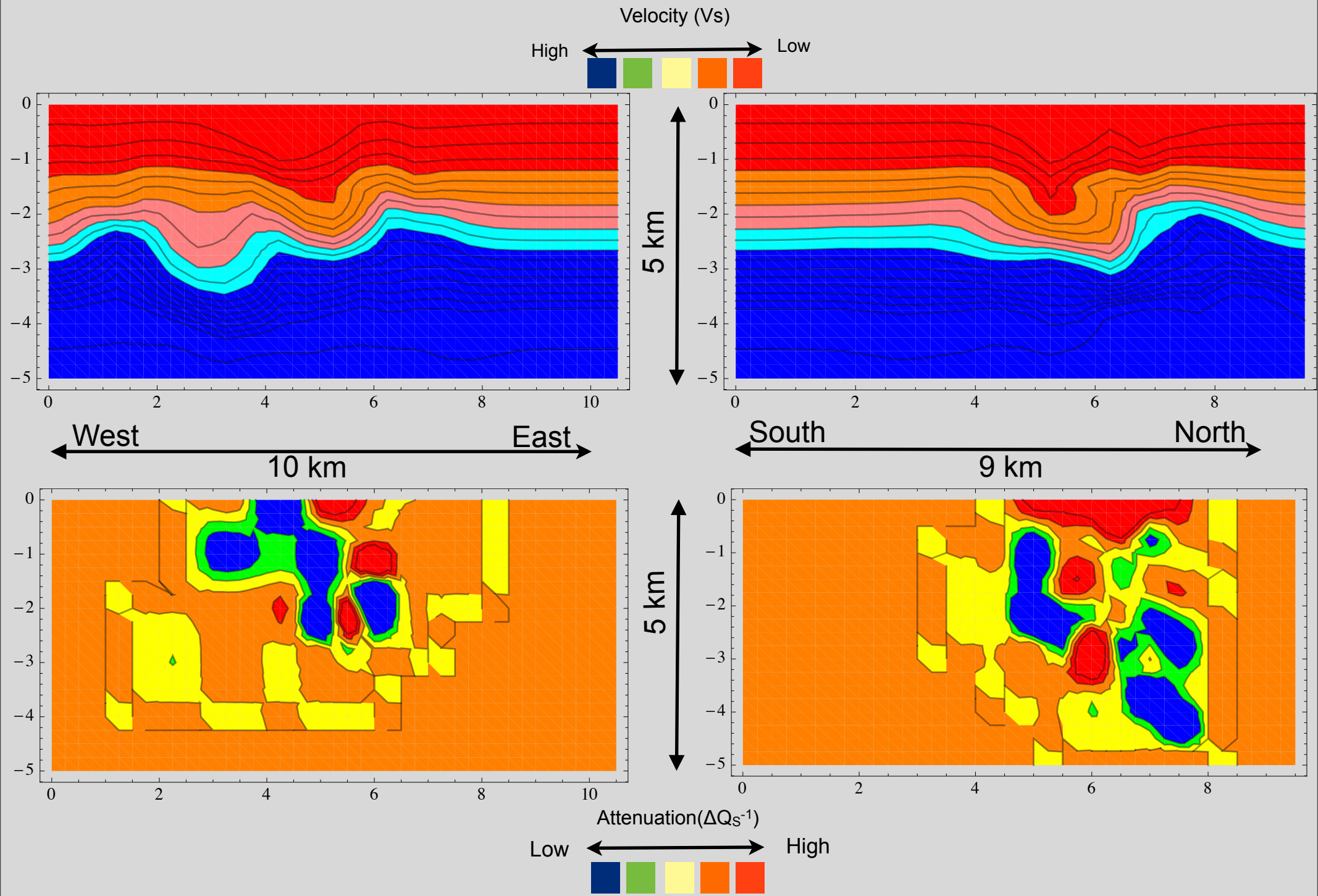

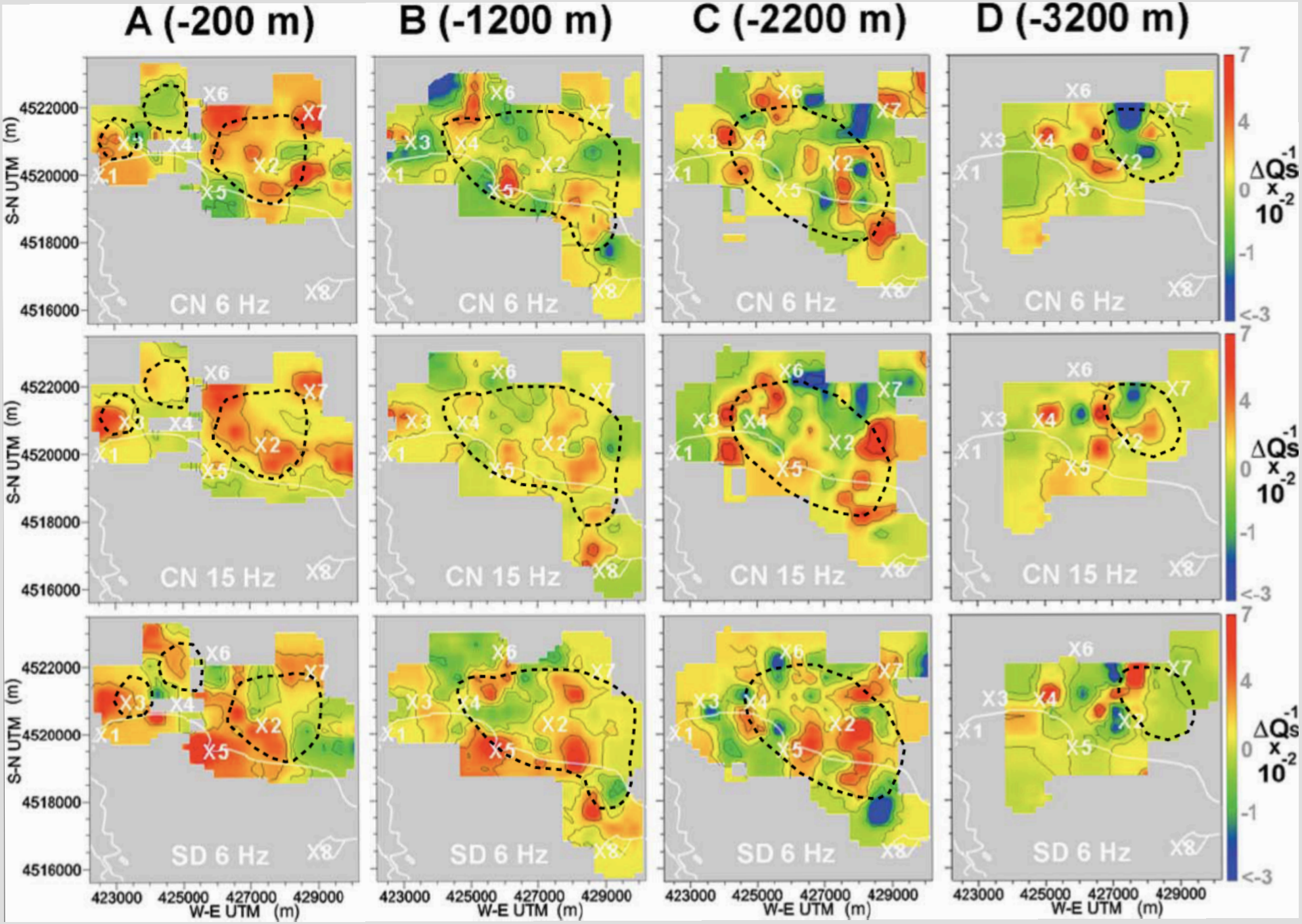

Results for S-wave attenuation- horizontal slices

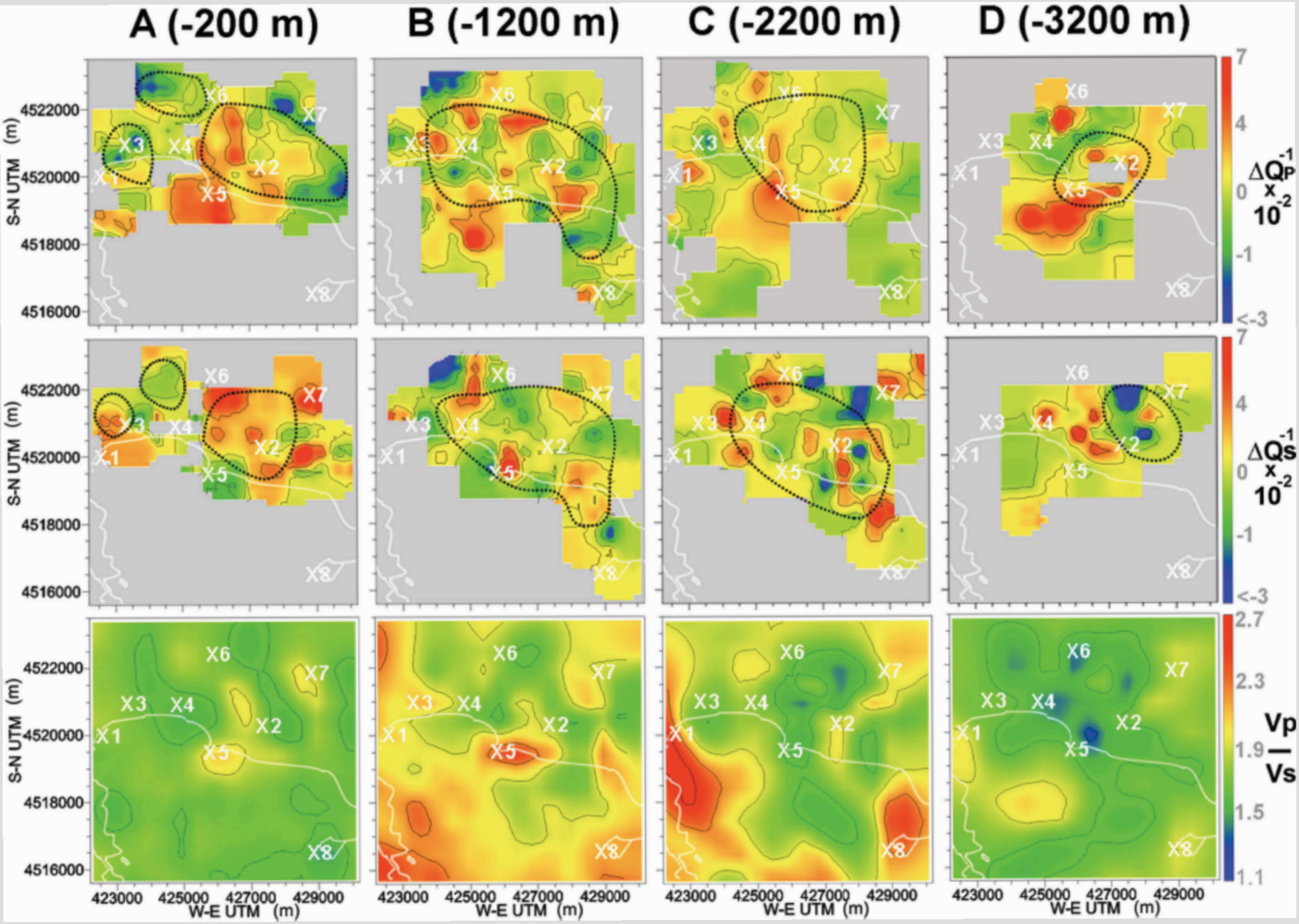

Attenuation(ΔQ_P^{-1})

Low ⟷ High

Results for P- and S-wave attenuation and Vp/Vs - horizontal slices

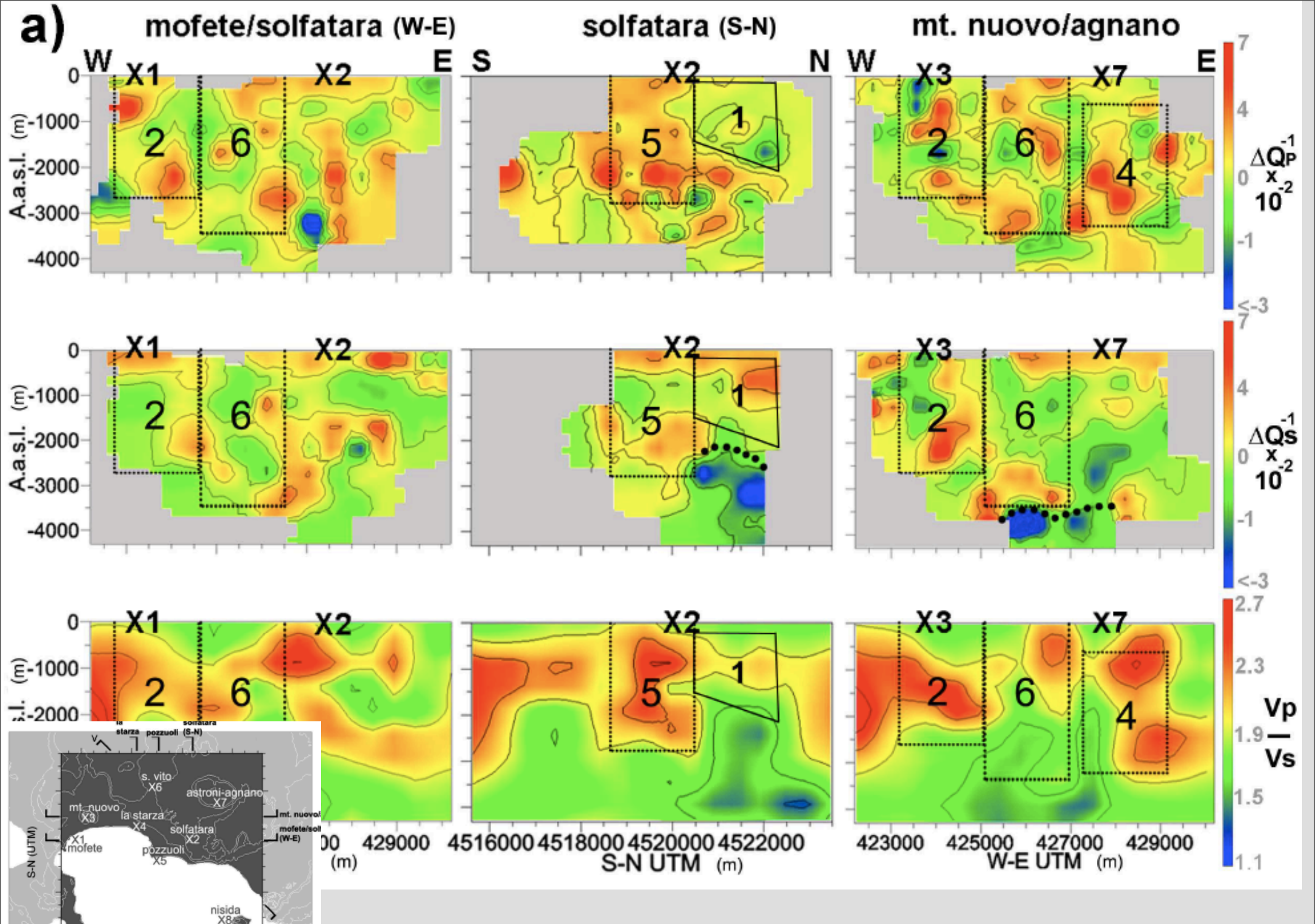

Results for P- and S-wave attenuation and Vp/Vs - Vertical sections

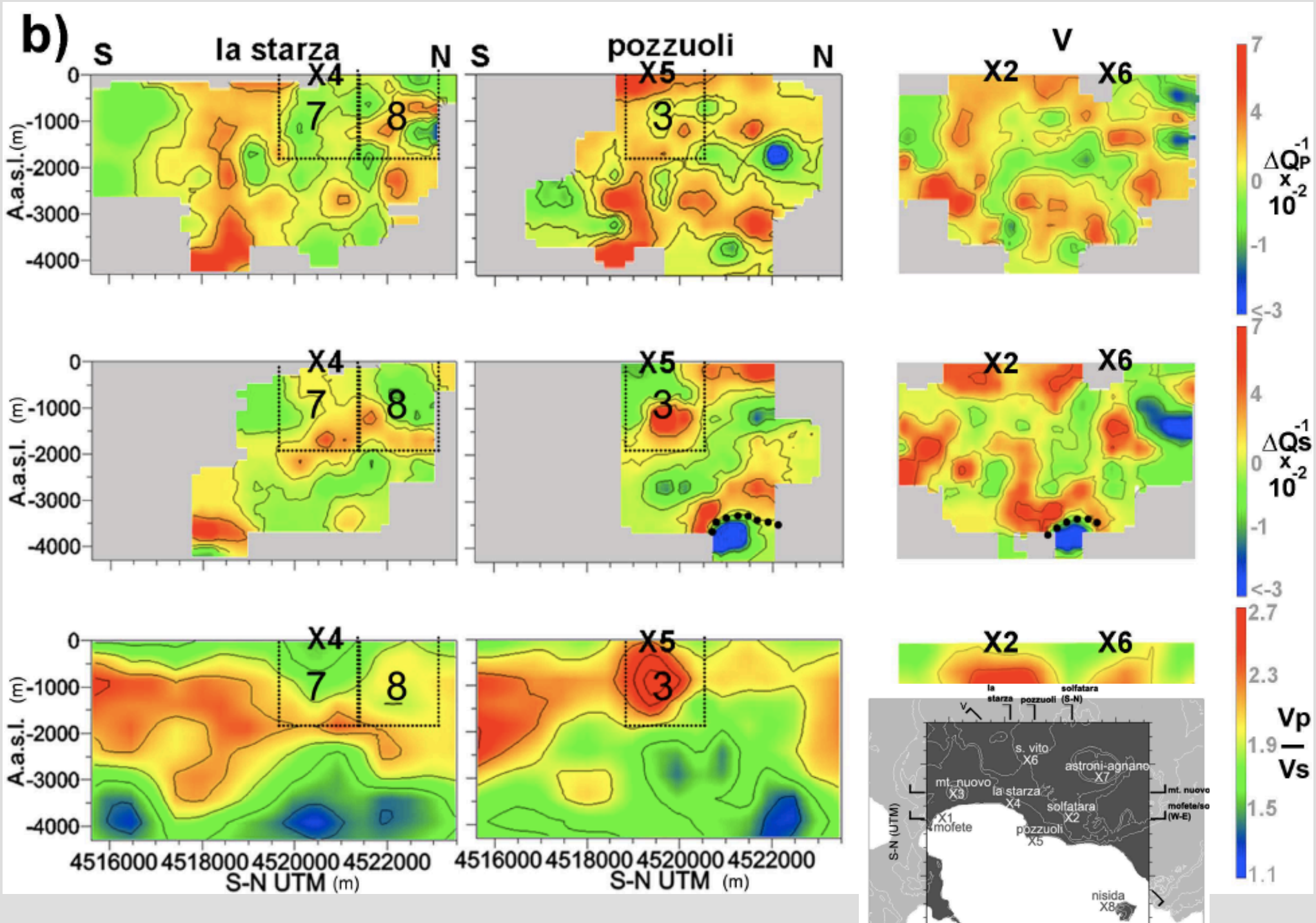

Results for P- and S-wave attenuation and Vp/Vs - Vertical sections

The seismological interpretation

V_P	V_S	Q_P^{-1}	Q_S^{-1}	V_P/V_S	Interpretation	Examples and bibliography
L	L	H	H	L	Fractured porous zone, typically on surface	Gudmundsson Ó., Finlayson D. M., Itikarai I., Nishimura Y., and Johnson W. R., 2004. Seismic attenuation at Rabaul volcano, Papua New Guinea. J. of Volc. and Geoth. Re., 130: 77-92.
H	?	H	?	?	Fractured zone, with the presence of fluids	De Gori, Chiarabba and Patanè, 2005. Qp structure of Mount Etna: Constraints for the physics of the plumbing system. JGR Vol 110
L	L	H	H	A/H	Magma, fluids	Schurr, B., Asch, G., Rietbrock, A., Trumbull, R., and Haberland, C., 2003. Complex patterns of fluid and melt transport in the central Andean subduction zone revealed by attenuation tomography. Earth. Pl. Scien. Lett., 215: 105-119.
L	L	H	L	L/A	Presence of gasses	Hansen, S., Thurber, C. H., Mandernach, M., Haslinger, F., and Doran, C., 2004. Seismic Velocity and Attenuation Structure of the East Rift Zone and South Flank of Kilauea Volcano, Hawaii. Bull. of the Seism. Soc. of Am., 94: 1430-1440.
H	H	L	L	A	Compact zone, tipically at high depth	Eberhart-Phillips, D., Reyners, M., Chadwick, M., Chiu, J. M., 2005. Crustal heterogeneity and subduction processes: 3-D VP, VP/VS and Q in the southern North Island, New Zealand. Geophys. J. Int. 162: 270--288.
H	?	L	?	?	Volcanic conduit	De Gori, Chiarabba and Patanè, 2005. Qp structure of Mount Etna: Constraints for the physics of the plumbing system. JGR Vol 110

Captions
L = Low
H = High
A = Average
? = Unknown

- the volumes below Mofete-Mt-Nuovo, Pozzuoli and Agnano are characterized by the presence of hydrothermal basins (Todesco et al., 2003, Vanorio et al., 2005)
- the volumes below San Vito and the North-Eastern Solfatara are characterized by the presence of small gas reservoirs (Todesco et al., 2003)
- the volumes below the point of maximum uplift in the 1983-1984 crisis and the La Starza fault are characterized by the presence of strong attenuation contrasts
- a seismic horizontal velocity and attenuation interface is clearly visible everywhere around Pozzuoli and Solfatara around -3000 m depth (Zollo et al., 2008)

A possible interpretation in terms of melt zones and gas-filled structures

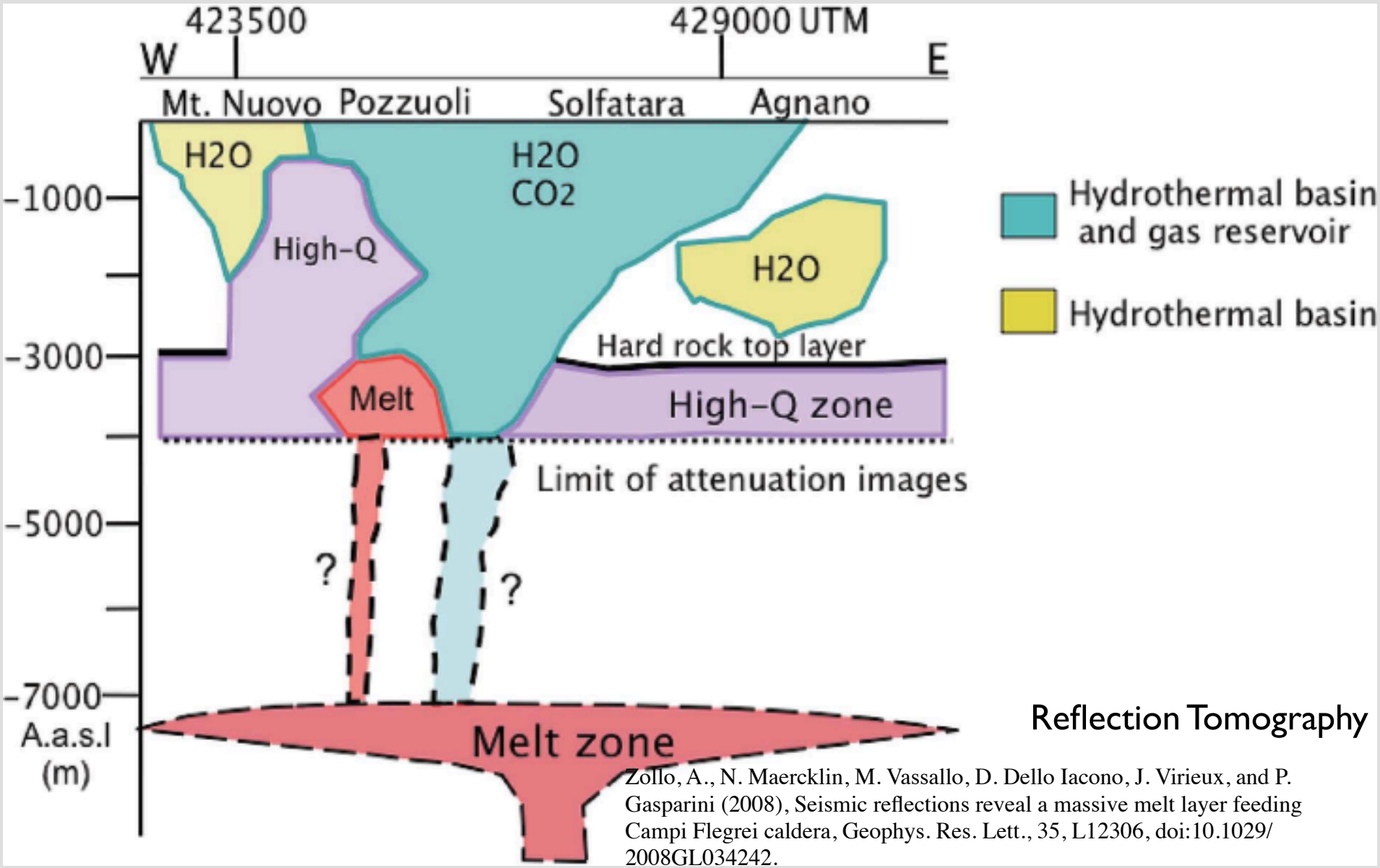

Zollo, A., N. Maercklin, M. Vassallo, D. Dello Iacono, J. Virieux, and P. Gasparini (2008), Seismic reflections reveal a massive melt layer feeding Campi Flegrei caldera, Geophys. Res. Lett., 35, L12306, doi:10.1029/2008GL034242.

Scattering tomography

$$E_u(\mathbf{x},t) = \frac{Wg_0}{V_0(4\pi)^2}\exp(-2\pi f t\, Q_C^{-1}) \sum_{i=1}^{Nscat} \delta\left(t - \frac{r_a(\mathbf{z}_i) + r_b(\mathbf{z}_i)}{V_0}\right) \frac{1}{r_a^2(\mathbf{z}_i) r_b^2(\mathbf{z}_i)}$$

Mean Energy in the Ellipsoidal shell

$$E_{nu}(\mathbf{x},t) = \frac{Wg_0}{V_0(4\pi)^2}\exp(-2\pi f t\, Q_C^{-1}) \sum_{i=1}^{Nscat} \delta\left(t - \frac{r_a(\mathbf{z}_i) + r_b(\mathbf{z}_i)}{V_0}\right) \frac{\alpha_i}{r_a^2(\mathbf{z}_i) r_b^2(\mathbf{z}_i)}$$

Adding explicitly scattering coefficients

For the k-th source and the m-th receiver, at the j-th lapse time along the coda

$$\frac{\epsilon_{nu}(\mathbf{x}_m)_{jk}}{\epsilon_u(\mathbf{x}_m)_{jk}} = a_{mjk} = \frac{\sum_{i=1}^{Nscat} (\alpha_i / r_{amk}^2(\mathbf{z}_i) r_{bmk}^2(\mathbf{z}_i))}{\sum_{i=1}^{Nscat} (1 / r_{amk}^2(\mathbf{z}_i) r_{bmk}^2(\mathbf{z}_i))}$$

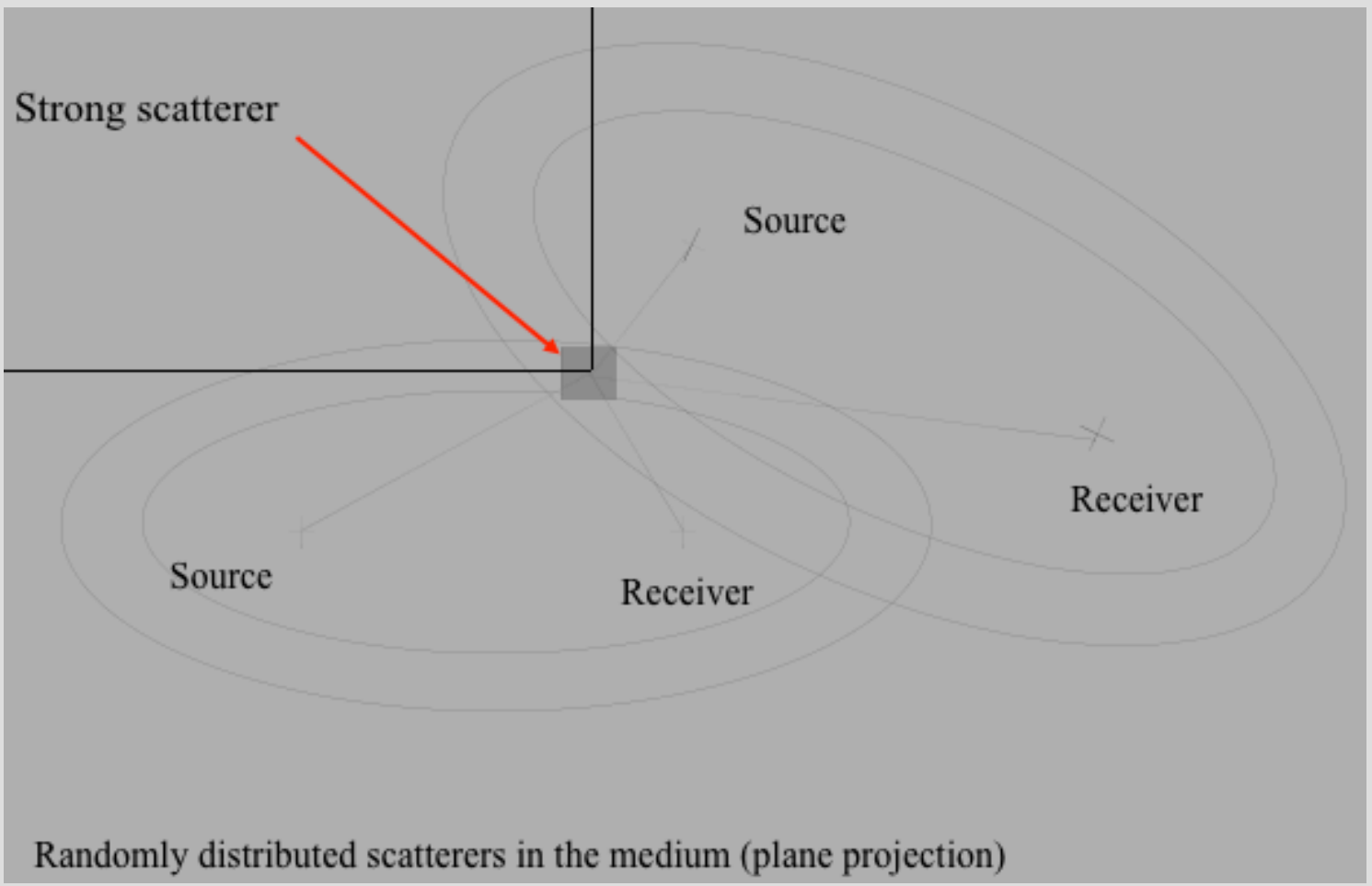

Scattering Imaging using passive data: coda waves

An example of data processing

The seismogram coda

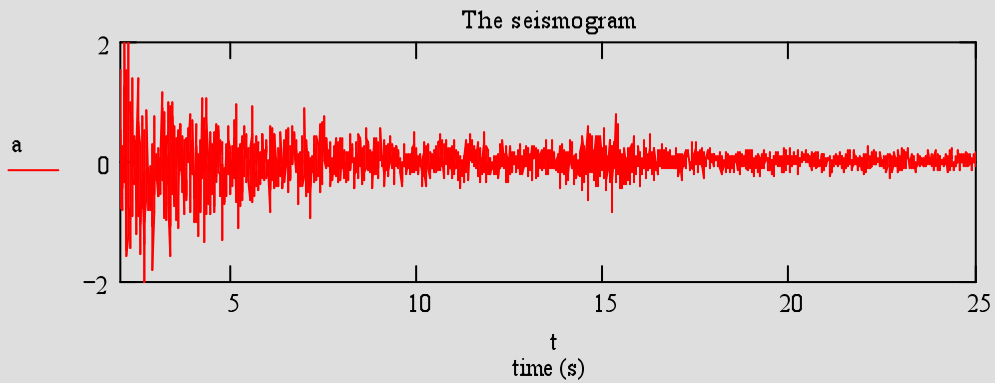

The seismogram coda envelope, and the theoretical envelope (blue). The black arrow indicate the effect of a strong scatterer

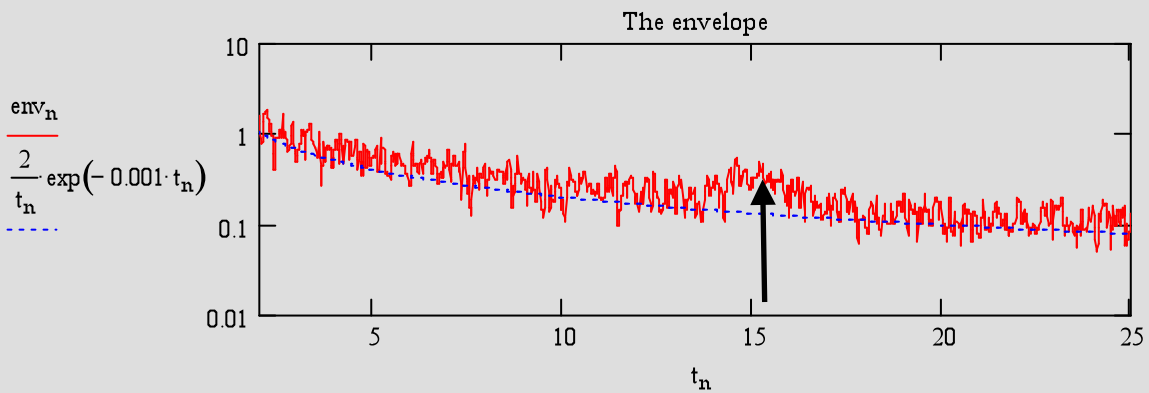

Residuals as a function of lapse time. These data form the seismic attributes to be inverted.

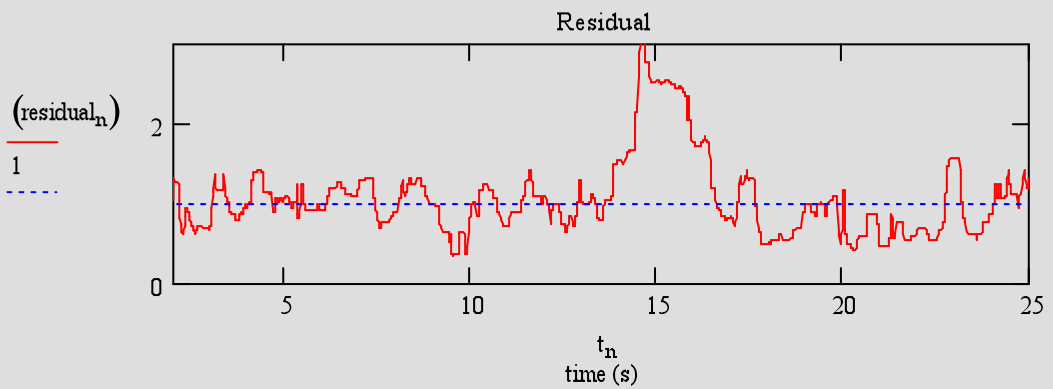

Scattering Image of Mt. Vesuvius

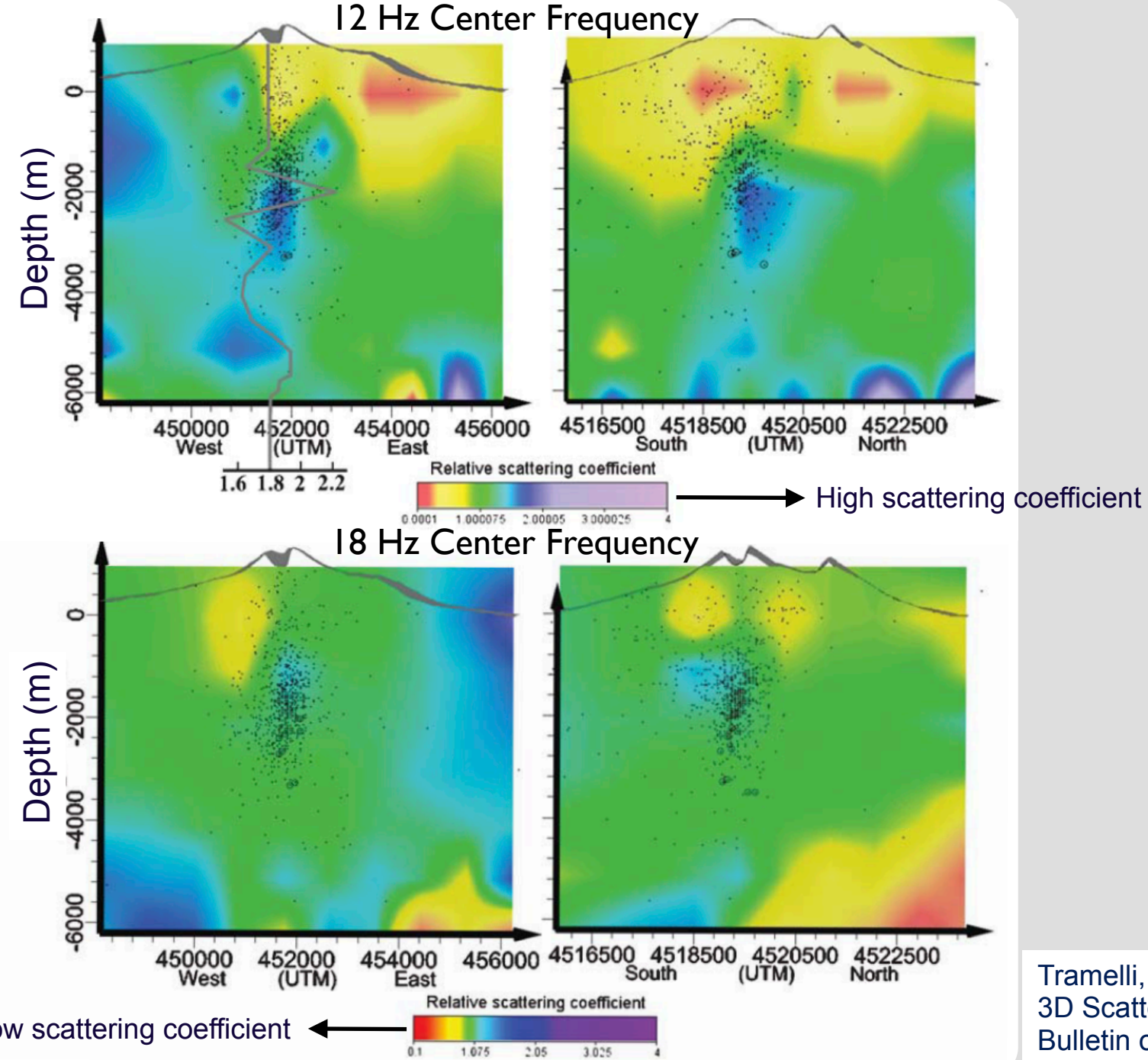

Tramelli, Del Pezzo and Fehler.
3D Scattering Image of Mt. Vesuvius.
Bulletin of the Seismological Society of America (2009).

Scattering Image of Campi Flegrei caldera.

The right 4 panels represent the attenuation tomography results in the same area

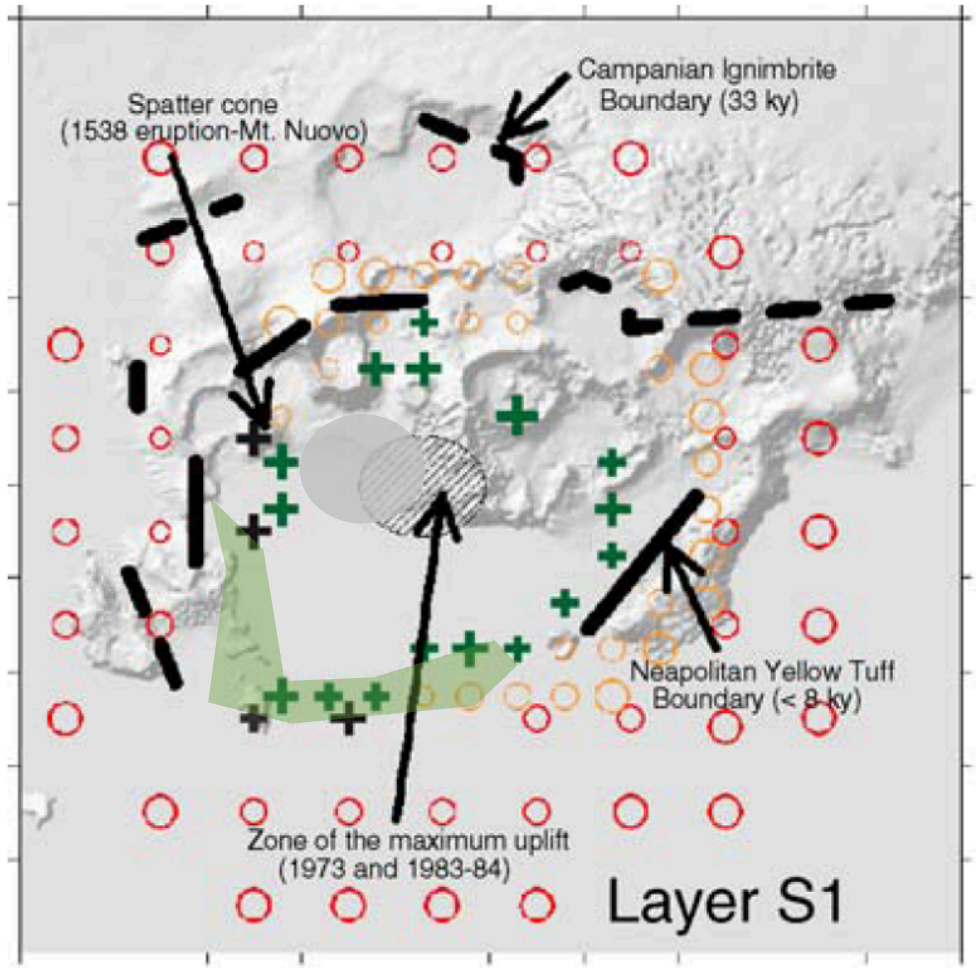

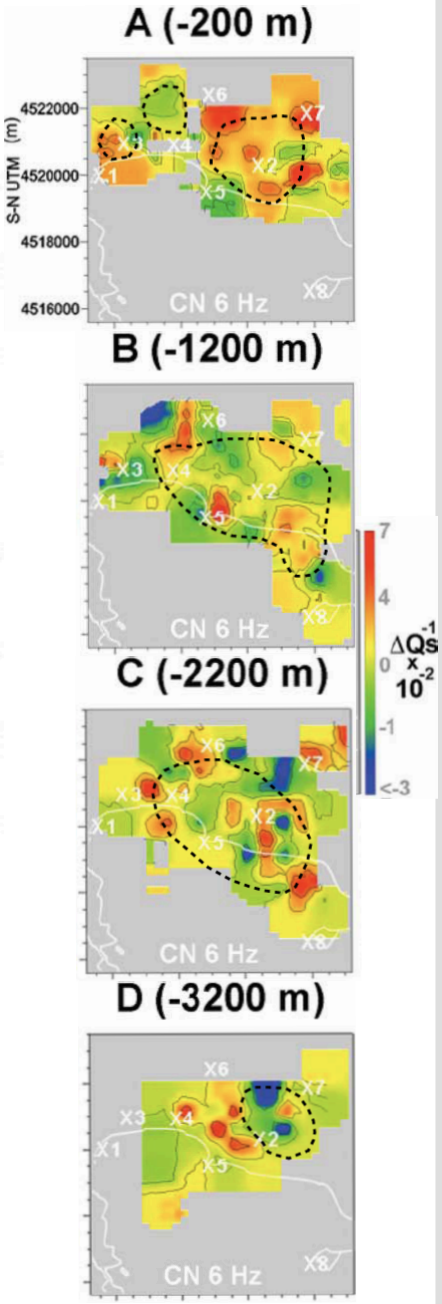

Outer caldera rim (Campanian ignimbrite)

Inner caldera rim (yellow tuff)

Max uplift zone (1983-84 bradiseism)

High P velocity contrast
(Zollo et al., 2003)

High Vp/Vs (Aster et al. 1989)

Tramelli, A., Del Pezzo, E., Bianco, F., Boschi, E. 3D scattering image of the Campi Flegrei caldera (Southern Italy). New hints on the position of the old caldera rim. Physics of the Earth and Planetary Interiors (2006)

Conclusions

- Images in velocity, attenuation and scattering are complementary
- Joint interpretation helps in determining the "lithology" of the volcano structures and to individuate the so called "magma chambers" when present
- Joint inversion of travel times and radiation spectra of direct and coda waves based onto a single overall equation linking these attributes to the lithological structure of a volcano, is the next challenge for volcano seismology.